Impact of glacial activity on the weathering of Hf isotopes - observations from Southwest Greenland

Jörg Rickli[a,b*], Ruth S. Hindshaw[c], Julien Leuthold[b], Jemma L. Wadham[d], Kevin W. Burton[e] and Derek Vance[b]

[a] Bristol Isotope Group, School of Earth Sciences, University of Bristol, Wills Memorial Building, Bristol BS8 1RJ, UK

[b] ETH Zurich, Institute of Geochemistry and Petrology, Clausiusstrasse 25, 8092 Zurich, Switzerland

[c] Department of Earth Sciences, University of Cambridge, Downing Street, UK, CB2 3EQ

[d] School of Geographical Sciences, University of Bristol, University Road, Bristol BS8 1SS, UK

[e] Department of Earth Sciences, Durham University, Science Labs, Durham, DH1 3LE, UK

* Corresponding author. Tel.: +41 44 632 35 62, E-mail address: joerg.rickli@erdw.ethz.ch

Further email addresses:

Ruth Hindshaw: rsh45@cam.ac.uk

Julien Leuthold: julien.leuthold@erdw.ethz.ch

Jemma Wadham: J.L.Wadham@bristol.ac.uk

Kevin Burton: kevin.burton@durham.ac.uk

Derek Vance: derek.vance@erdw.ethz.ch

Abstract Data for the modern oceans and their authigenic precipitates suggest incongruent release of hafnium (Hf) isotopes by chemical weathering of the continents. The fact that weathering during recent glacial periods is associated with more congruent release of Hf isotopes has led to the hypothesis that the incongruency may be controlled by retention of unradiogenic Hf by zircons, and that glacial grinding enhances release of Hf from zircons. Here we study the relationship between glacial weathering processes and Hf isotope compositions released to rivers fed by land-terminating glaciers of the Greenland Ice Sheet, as well as neighbouring non-glacial streams. The weathered source rocks in the studied area mostly consist of gneisses, but also include amphibolites of the same age (1.9 Ga). Hafnium and neodymium isotope compositions in catchment sediments and in the riverine suspended load are consistent with a predominantly gneissic source containing variable trace amounts of zircon and different abundances of hornblende, garnet and titanite.

Glacially sourced rivers and non-glacial streams fed by precipitation and lakes show very unradiogenic Nd isotopic compositions, in a narrow range (ε_{Nd} = -42.8 to -37.9). Hafnium isotopes, on the other hand, are much more radiogenic and variable, with ε_{Hf} between -18.3 and -0.9 in glacial rivers, and even more radiogenic values of +15.8 to +46.3 in non-glacial streams. Although relatively unradiogenic Hf is released by glacial weathering, glacial rivers actually fall close to the seawater array in Hf-Nd isotope space and are not distinctly unradiogenic.

Based on their abundance in rocks and sediments and their isotope compositions, different minerals contribute to the radiogenic Hf in solution with a decreasing relevance from garnet to titanite, hornblende and apatite. Neodymium isotopes preclude a much stronger representation of titanite, hornblende and apatite in solution, such as might result from differences in dissolution rates, than estimated from mineral abundance. The strong contrast in Hf isotope compositions between glacial rivers and non-glacial streams results mostly from different contributions from garnet and zircon, where zircon weathering is more efficient in the subglacial environment.

A key difference between glacial and non-glacial waters is the water-rock interaction time. While glacial rivers receive continuous contributions from long residence time waters of distributed subglacial drainage systems, non-glacial streams are characterized by fast superficial drainage above the permafrost horizon. Therefore, the increased congruency in Hf isotope weathering in glacial systems could simply reflect the hydrological conditions at the base of the ice-sheet and glaciers, with zircon weathering contributions increasing with water-rock interaction time.

1. Introduction

Glacial weathering processes promote high silicate weathering rates over Pleistocene glacial-interglacial cycles (e.g., Vance et al., 2009). Glacial grinding of rock substrate produces fine-grained rock powder with large surface area, which can be exposed to weathering in a range of settings (e.g., Anderson, 2007). In addition to surface area, soil age is an intrinsic factor for silicate-weathering rates, with rates decreasing rapidly with time of exposure (e.g., Taylor and Blum, 1995). Taken together, glacial-interglacial cycles combine to yield high time-integrated silicate weathering rates as reactive soil substrate is produced during glacial periods and weathered effectively in intervening interglacials (Foster and Vance, 2006). These interactions may be reflected in the Pb isotope evolution of seawater in the northwestern Atlantic (Foster and Vance, 2006; Gutjahr et al., 2009; Kurzweil et al., 2010). Other approaches to study variations in glacial-interglacial weathering rates, such as oceanic $^{10}Be/^{9}Be$ ratios, on the other hand, suggest little change (von Blanckenburg et al., 2015).

Continental weathering conditions also affect the seawater evolution of Hf isotopes on Pleistocene and longer time-scales (Piotrowski et al., 2000; van de Flierdt et al., 2002; Gutjahr et al., 2014; Dausmann et al., 2015; 2017). These variations can, however, also reflect changes in weathered source rocks rather than the degree of weathering congruency (Chen et al., 2012). The information Hf isotopes hold has not been fully accessible to date due to our limited understanding of their behaviour during weathering. Early studies of iron-manganese crusts and nodules, which record ambient seawater isotope

compositions for radiogenic isotopes, suggested that the generally incongruent release of Hf isotopes during weathering is diminished during times of continental glaciation (Piotrowski et al., 2000; van de Flierdt et al., 2002). A cause for the incongruency of Hf isotope release is the retention of unradiogenic Hf isotopes in weathering-resistant zircon (Patchett et al., 1984), with more efficient release during glacial times due to glacial comminution of rocks and the production of glacially strained surfaces (Piotrowski et al., 2000; van de Flierdt et al., 2002). This concept has recently been reinforced by observations on the Hf isotope composition in dispersed marine iron-manganese phases extracted from sediments that span the last deglaciation of North America (Gutjahr et al., 2014). In addition, Gutjahr et al. (2014) inferred that a change from a relatively congruent release of Hf isotopes during the Last Glacial Maximum to a more incongruent release shortly afterwards could be linked to the transition from a dominantly cold-based to a warm-based Laurentide Ice Sheet.

A complementary mineralogical control, namely the release of radiogenic Hf from preferentially weathered accessory minerals with high Lu/Hf ratios, can also affect the incongruency in Hf isotope weathering (Bayon et al., 2006; Godfrey et al., 2007; Chen et al., 2011; 2013a,b). Thus, studies of the dissolved load of rivers specifically invoke preferential weathering of apatite and titanite or garnet, depending on the weathering lithologies (Bayon et al., 2006; Godfrey et al., 2007). Hafnium released during weathering may, hence, become more congruent with increasing soil age, as the accessory minerals are depleted. This mechanism has, however, not been evaluated conclusively to date (e.g., Ma et al., 2010; Bayon et al., 2016). An effect on dissolved Hf from the dissolution of radiogenic accessory minerals, which also carry radiogenic Pb, appears to be at odds with observations from the North Atlantic as there is no co-evolution of seawater Pb and Hf - isotope compositions (Gutjahr et al., 2014).

In addition to glacial activity, mineralogy and soil age, the release of Hf isotopes has also been suggested to depend on run-off conditions and temperature (Bayon et al., 2012; 2016; Rickli et al., 2013). High run-off seems to promote the release of radiogenic Hf, as observed in catchments with different source lithologies in Switzerland (Rickli et al., 2013). Hafnium

isotopes in the clay fraction of river and shelf sediments, mostly reflecting released Hf during weathering, are positively correlated with precipitation and temperature in catchments of various sizes and lithology from around the globe (Bayon et al., 2016).

A currently unclear aspect of seawater Hf isotope compositions is the relative overall homogeneity between ε_{Hf} = -2 in the Northwest Atlantic and ε_{Hf} = +6 in the North Pacific (Rickli et al., 2009; Zimmermann et al., 2009a). This narrow range cannot be easily reconciled with the variable riverine Hf isotope compositions reported thus far (Bayon et al., 2006; Godfrey et al., 2007; Chen et al., 2013b; Rickli et al., 2013; Merschel et al., 2017) and a short seawater residence time of Hf (Chen et al., 2013b; Filippova et al., 2017), similar to that of Nd (< 500 yr, Siddall et al., 2008).

In summary, the interplay of environmental parameters – such as soil age, glacial activity, temperature and precipitation - and mineralogical properties of weathered rocks – in particular the availability of specific accessory minerals - is likely to govern the Hf isotope compositions of rivers. But the relative significance of these aspects is not well constrained to date. In this study, we seek to characterise the hydrological and mineralogical controls on the congruency in Hf isotope release in the subglacial and proglacial environment of the Russell and Leverett Glaciers in West Greenland (Fig. 1). To this end, we have characterized the weathered source rocks and derived sediments, and compare them to the dissolved riverine isotope compositions, specifically in glacially fed rivers and non-glacial streams.

2. Study area

The studied rivers and streams are situated within the proglacial zone of the Greenland Ice Sheet (GRIS), inland from Søndre Strømfjord, near the town of Kangerlussuaq on the west coast of Greenland (Fig. 1). Glacial waters were sampled in July 2006 from the two major rivers in the region, Akuliarusiarsuup Kuua and Quinnguata Kuusua, which merge at Kangerlussuaq to form the Watson River. In addition, four non-glacial streams (GR11, 12, 13 and 15) and a further glacial stream (GR9) were sampled. A time series of 11 different samples was obtained from the main river draining Leverett Glacier in July

2009 (Table 1). For the purpose of this study, glacial rivers refer to those that are directly fed by ice sheet melting, as opposed to non-glacial streams, which are not directly linked to the ice sheet. The discharge of the latter is derived from direct precipitation as well as drainage from shallow lakes, which make up 5–10% of the surface area around Kangerlussuaq (Willemse, 2002).

The study area is dominated by amphibolite facies gneisses belonging to the Ikertôq complex of the Nagssugtoqidian fold belt. The protoliths initially formed at 3 to 2.7 Ga and were metamorphosed at 1.9 Ga (Fig 1., Henriksen et al., 2000). Amphibolite layers and lenses within the gneisses are thought to represent metamorphosed remnants of dolerite dykes (Escher et al., 1976). To the southeast, the Nagssugtoqidian fold belt is bordered by the Archean Craton of Greenland, where a felsic intrusion related to the Qôrqut granite (2.5 Ga) and granulite facies gneisses outcrop (Henriksen et al., 2000). Although the felsic intrusion may be of some relevance as a source lithology for weathering at, for example, the Leverett site (see section 5.4), this is unlikely to be the case for the cratonic gneisses given their spatial occurrence (Fig. 1).

The area is characterized by an Arctic climate with a mean annual temperature of -5.7 °C (1973-1999). Seasonal variations are pronounced, with an average of -19.8 °C in January and of +10.7 °C in July (Cappelen et al., 2001). Annual precipitation amounts to only 149 mm (1973-1999, Cappelen et al., 2001), compared to 300 mm of evapotranspiration (Hasholt and Sogaard, 1978). In the unglaciated area permafrost is continuous, with an active layer thickness of 0.1–2.5 m (Tatenhove, 1996). Most of the deglaciated area of the study has been ice-free since at least ~6.8 ka (Fig. 1, Levy et al., 2012 and references therein). The non-glacial streams GR11, 12 and 13 are situated to the west of the Ørkendalen moraines. These moraines delimit the largest areal extent of the GRIS between ~6.8 ka and the late 19th century, at a distance < 2 km from the current Ice Sheet margin. Stream GR15, flowing eastwards from a non-glacial lake to a small lake with glacial inflow, drains sediments very close to the Ice Sheet margin (see Fig. 2a in Levy et al., 2012). This stream is, however, mostly within the Ørkendalen moraines and, therefore, probably not influenced by the weathering of more recently exposed glacial material.

Recent studies have indicated that the Leverett and Russell Glaciers experience strong seasonal variations in subglacial hydrology similar to those observed in smaller alpine glaciers, whereby an inefficient distributed drainage network transforms into an efficient channelized network of drainage channels as the summer progresses (Bartholomew et al., 2010; Chandler et al., 2013). Such changes have also been observed in other outlet glaciers of the GRIS, suggesting that they are a common feature (Bhatia et al., 2011; Palmer et al., 2011; Meierbachtol et al., 2013).

3. METHODS

3.1. Water and solid samples

3.1.1 Glacial rivers (excluding Leverett River) and non-glacial streams

Both glacial and non- glacial samples were collected in July 2006 (Fig. 1, Table 1). Previous studies have reported Li and Mg isotope compositions of these samples, also providing data on sediment load, river chemistry, pH and temperature (Wimpenny et al., 2010; 2011). Some of the glacially fed rivers were sampled far from the ice sheet, and thus receive small contributions from non-glacially sourced waters (e.g., GR2, GR7, Fig. 1) with limited effects on glacial river chemistry. Some of the non-glacial samples were coloured (GR11 and GR12), possibly reflecting high organic contents. Sample GR10 was taken close to the harbour and contains a significant seawater component.

At each sample location approximately 15 l of river water were collected for Hf and Nd isotope analysis. Each water sample was filtered (0.2 μm) within 12 h of sampling using a Sartorius frontal filtration unit. Suspended particulate material was also kept for analysis. Hafnium and neodymium were subsequently enriched from the water by co-precipitation with Fe (e.g., Rickli et al., 2009).

3.1.2 Leverett Glacier time series

The main river draining the Leverett Glacier was sampled 11 times between the 6th and the 28th of July 2009 (Table 1, Fig. 1). Samples were taken every second day (excluding the 16th of July), alternating between ~8:30 and ~17:30 local time. The sampling location was ~1 km downstream from the glacier

mouth, in a stretch of turbulent flow (Fig. 1). Hence, samples taken at the edge of the river are considered representative of the bulk water chemistry. In addition, water samples were taken from a proglacial lake close to the river sampling site, as well as from two supraglacial streams.

Water samples were collected in acid-cleaned 15 l HD-PE carboys pre-rinsed with river water. Samples were filtered (0.45 µm) within 24 hours of sampling using a peristaltic pump, clean HD-PE tubing and a filter holder made from polypropylene. A second filtration was performed after the initial filtration to ensure complete removal of suspended load in this high suspension river (> 2 g/l, see section 4.1). An unfiltered aliquot of Leverett River samples was kept to determine Hf and Nd isotope compositions and concentrations in the suspended sediment load. This, however, implied small but well constrained corrections for the measured isotopes to account for dissolved elemental contributions (<0.02 εNd, <0.2 ε_{Hf}). Dissolved Nd and Hf for isotope analysis were enriched from 10 to 20 l of filtered water by co-precipitation with Fe (e.g., Rickli et al., 2009). A separate 1 l aliquot was kept for elemental analysis (Hf, Sm, Nd) and acidified to pH < 2 with double distilled HCl.

Complementary data - including pH, temperature, runoff, suspended sediment amounts, solute concentrations and Sr/Ca isotope data - have previously been published (Bartholomew et al., 2010; Hindshaw et al., 2014). This data is used here to characterize river chemistry and hydrological conditions.

3.1.3 Solid samples

Hafnium and neodymium isotopes and concentrations (Sm, Nd, Hf by isotope dilution) have been measured on undissolved sample aliquots from Hindshaw et al. (2014). These samples include: (i) powders of two orthogneisses (Ro2, Ro4), two amphibolites (Ro1, Ro3) and 17 mineral separates of these rocks, which were collected close to the sampling location on the Leverett River (Fig. 1); (ii) seven sediments from the proglacial environment of Leverett Glacier, including the river bank at the dissolved load sampling location (Sed 1, 2; LC sand), a side moraine (SM Sed), a proglacial lake (PGL 1) and dirt cones on Leverett Glacier (MH 1, 2, Fig. 1). Note that, to avoid confusion between the

notation of Wimpenny et al. (2010) and Hindshaw et al. (2014), the rock samples of Hindshaw et al. (2014) are relabelled from GRO1 to Ro1, etc.

In addition, Hf and Nd systematics were measured for two zircon separates from Ro2 and Ro4, a rutile separate from Ro3 and four garnet and one apatite separate from catchment sediments (Table 2). Measurements of suspended particulate matter from the Leverett River, Akuliarusiarsuup Kuua and Quinnguata Kuusua, and a bulk rock analysis of an Archean granite sample originating from southwest of Quinnguata Kususa (ggu 415961, Fig. 1), complement the data.

Mineral separates were obtained from the < 425 µm fraction using heavy liquids and magnetic separation to enrich minerals, followed by handpicking under a binocular microscope (see Hindshaw et al., 2014). The separates, excluding apatite, were initially leached for 30 minutes in 6M HCl at 80°C to remove potential surface contamination, and subsequently rinsed twice with MQ. All solid samples, except the zircon and apatite separates, were digested on a hotplate at 120 °C for at least two days in a mixture of concentrated HF and HNO_3 (28 M, 14 M, 4:1). Zircons were leached in the same mixture for four hours and the weight loss was monitored to calculate elemental concentrations. The apatite separate was dissolved in 7M HNO_3 to avoid digestion of silicate inclusions.

After evaporation to dryness, all solid samples were repeatedly dissolved and dried in 6M HCl to eventually yield clear solutions in 6ml of 6M HCl. Isotope compositions (Hf, Nd) and elemental concentrations by isotope dilution (Hf, Sm and Nd) were usually obtained on separate fractions of these stock solutions. In the case of minerals, however, Sm/Nd concentrations as well as Hf and Nd isotopes were obtained on the same solution fraction (spiked with a tracer enriched in ^{150}Nd and ^{149}Sm), whereas Hf concentrations were determined separately.

3.2. Ion chromatography and procedural blanks

Ion chromatographic procedures for the purification of Hf and Nd followed previously detailed methods (Rickli et al., 2009; 2013) based on earlier work (Patchett and Tatsumoto, 1980; Pin and Zalduegui, 1997; Münker et al., 2001).

Total procedural blanks amount to < 30 pg of Hf and Nd for the procedures used for isotope measurements, and to < 2 pg and < 7 pg for concentrations. Average blank levels for Hf and Nd isotope measurements were < 0.05% of the sample sizes. Some trace element poor mineral separates had elevated blank contributions of 0.2 - 0.5% for Hf and 0.1 - 0.3% for Nd. The procedural blank for Nd concentrations was < 0.1%. In the case of Hf concentrations, it was < 0.1% for solid samples, but ranged between 0.3 and 1% for waters. No blank corrections were applied to isotope and concentration data.

3.3. Elemental concentrations of Hf, Sm and Nd

Elemental concentrations of Hf, Sm and Nd for river waters, and hotplate digests of solid samples, were measured by isotope dilution following previously outlined methods (Rickli et al., 2009; Table 1, 2). Reproducibility of Sm, Nd and Hf concentrations by isotope dilution was better than 1% for river waters and rocks (replicate measurement of Lev10 and BCR-2). Samarium/neodymium ratios reproduced to within 0.3 ‰.

Hafnium concentrations were also measured by isotope dilution on di-Lithium tetraborate fused rock powders and catchment sediments. Major elements - Si, Al, Fe, Ti, Ca, Mg, K, Na, P, Mn - and Sr concentrations for these fused samples were presented in Hindshaw et al. (2014). Fusion will completely dissolve highly resistant minerals like zircon, whereas they can remain largely unaffected during hotplate digestion.

Individual mineral grains in sediments from the proglacial environment of Leverett Glacier (Fig. 1b) were also analysed for trace elements by LA-ICP-MS using a Thermo Element XR connected to a 193 nm Resonetics ArF Excimer laser (ETH Zurich). Some of these sediments were collected from the same sites as in Hindshaw et al. (2014), although they represent separate sample aliquots. Coordinates of sampling locations and further details are given in Appendix S1. Sediments were mounted in EPOXY blocks and polished to 1 μm. The laser was operated in a Laurin Technic S155 ablation cell with a spot size between 20 and 43 μm, a frequency of 4-5 Hz and a laser power density of 2 J/cm^2. Electron microprobe (EMP) data were used as internal standards for all measured minerals. NIST SRM610 was used for external standardisation and

GSD-1G glass as a secondary standard (Jochum et al., 2011a; 2011b). Raw data were reduced off-line using the SILLS software (Guillong et al., 2008). Uncertainties, on repeat measurements of GSD-1G at concentrations of 40-50 ppm, usually range between 2 and 3% and are < 6% for all elements. For the low Hf and Nd concentrations in many of the analysed minerals, uncertainties are < 20 % at 5 ppm and up to 100 % close to the limit of detection (0.01 - 0.4 ppm). Trace element concentrations are given in Appendix S1.

3.4. Isotope analysis of Hf and Nd

Hafnium and neodymium isotopes were measured by MC-ICP-MS, either at the University of Bristol (Neptune) or at ETH Zurich (Neptune Plus). Instrumental mass bias correction followed Vance and Thirlwall (2002) in the case of Nd, and used a natural $^{179}Hf/^{177}Hf$ ratio of 0.7325 for Hf. The external reproducibility of the mass spectrometric analysis was monitored in each session by repeated measurements of La Jolla for Nd and JMC 475 for Hf (n ≥ 15), and the measured averages were used to renormalize the sample data to the respective literature values (Nowell et al., 1998; Thirlwall, 1991). For Nd isotopes, measured at concentrations > 50 ppb in most cases, external reproducibility is < 0.2 ε_{Nd} (2 SD). For Hf isotopes external reproducibility depends on available Hf for analysis, varying between < 0.3 ε_{Hf} for rocks, sediments and many minerals, to 0.5 - 0.6 ε_{Hf} for most riverine dissolved and suspended sediment samples. Internal errors were ≤ 0.6 ε_{Hf} for all but 6 samples (2 SEM, Table 1). More details of the uncertainties in Hf isotopic determination are given in Appendix S2, leading to the general conclusion that internal and external errors are, to a good approximation, identical for Hf isotopes.

Hafnium and neodymium isotopic compositions are expressed in epsilon units, as deviations from the Chondritic Uniform Reservoir (Jacobsen and Wasserburg, 1980; Bouvier et al., 2008).

3.5. Mineral abundances

Mineral abundances were obtained by point counting on thin section microphotographs combined with SEM back- scattered images and EDS

element maps using the ImageJ software. SEM analyses were carried out at the University of Bristol (Hitachi S-3500N microscope equipped with Thermo Noran energy dispersive spectrometer) and at ETH Zurich (Jeol JSM-6390LA instrument equipped with Thermo Fisher Ultradry EDS detector coupled to a Thermo Fisher Noran System 7).

4. Results

4.1. Hydrochemistry

Hydrochemical data, including runoff from Leverett Glacier in July 2009 (Fig. 2), have previously been published and discussed (Wimpenny et al., 2010; Bartholomew et al., 2011; Hindshaw et al., 2014). The key results relevant for the discussion of the new data on Hf and Nd isotopes are briefly summarized here.

The discharge of Leverett Glacier varied strongly during summer 2009 (Fig. 2), reflecting seasonal variation in insolation and corresponding surface ice melt. Discharge from Leverett Glacier was < 6 m^3/s prior to the start of June and then increased to a maximum value of 317 m^3/s on 16th July, before gradually declining again to 42 m^3/s on 3rd September (Bartholomew et al., 2011). Four distinct discharge pulses punctuate the rising limb of the hydrograph, coinciding with transient increases in suspended sediment concentrations and electrical conductivity. The last pulse started on 3rd July, just before the samples from this study were collected (Fig. 2, the first three discharge pulses are not shown). The discharge pulses have been linked to the sudden drainage of lakes on the glacier surface, which are known from satellite observations (Bartholomew et al., 2011). No discharge data are available for the other reported glacial and non-glacial samples.

Total dissolved solids (TDS), calculated as the sum of major cations (Ca, Mg, Na, K), major anions (HCO_3^-, SO_4^{2-}, Cl^-) and Si, show clear differences for glacial rivers versus non-glacial streams (Table 1). Glacial waters yield values between 160 and 470 µmol/l. In contrast, non-glacial streams yield much higher values between 851 and 5043 µmol/l, more similar to the lake (TDS = 8273 µmol/l). Total suspended sediment (TSS) ranges between 2.3 and 7.4 g/l in Leverett River and between 0.4 and 0.8 g/l in all other glacial samples. In

contrast, it is very low in non-glacial streams (< 0.014 g/l) due to calm water flow. From field observations it is also clear that lake and supraglacial waters are virtually suspension free, although no measurements are available.

Calcium/sodium ratios are low in all river samples, ranging between 0.6 and 3.9 (all ratios are reported on a molar basis, Table 1), indicating relatively small contributions from carbonate weathering (e.g., Gaillardet et al., 1999). Elevated K is characteristic of glacial samples, as observed before (e.g., Anderson et al., 1997), resulting in K/Na ratios of 0.54 to 1.22 compared to ratios between 0.03 and 0.48 in non-glacial samples. Magnesium, on the other hand, is more abundant in non-glacial streams, which define a relatively distinct field in major cation compositions (Fig. 3a). Bicarbonate is the dominant anion, contributing a mole fraction > 0.83 in glacial and 0.67-0.84 in non-glacial samples (Fig. 3b). Chlorine fractions are elevated in non-glacial streams, which also leads to a clear distinction of glacial and non-glacial water based on anions. Overall, the major cation and anion chemistry of the lake is similar to the non-glacial streams. All waters are under-saturated with respect to most minerals except, depending on the river or stream, in iron oxides and a few schist silicates (kaolinite, K-mica) (Wimpenny et al., 2010; Hindshaw et al., 2014).

4.2. Dissolved hafnium and neodymium

Concentration data are only available for the Leverett time series. Hafnium and neodymium concentrations are highest at the start of the sampling campaign, at the time of the meltwater pulse, yielding concentrations of 42.7 and 4984 pmol/l, respectively. The concentrations of both elements are negatively correlated with discharge reflecting dilution by increased meltwater over the course of the season (r = -0.86, Table 1, Fig. 2). Concentrations of many elements also show diurnal cycles due to increasing runoff over the course of the day (Hindshaw et al., 2014). Hafnium isotopes from the Leverett River show strong variability among the first three observations, between ε_{Hf} = -18.3 and -9.1. Subsequently they are relatively constant, in the range of -12.4 to -9.9 (Fig. 2). Further glacial samples overlap with the observations from Leverett

River, but also show more radiogenic signatures up to -0.9. Non-glacial streams are distinctly more radiogenic in Hf with values of +15.8 to +46.3 (Fig. 4a).

Dissolved Nd isotopes are essentially invariant in the Leverett River at ε_{Nd} = -38.5, within the range observed for other glacial samples (ε_{Nd} = -39.5 to -38, Table 1). Non-glacial streams are more heterogeneous (-42.8 to -38.7). Stream GR14 from close to Sisimut (see Fig. 1 inset) is not included in these isotope ranges for Hf and Nd, as its dissolved Nd isotope composition suggests drainage of somewhat different source lithologies (ε_{Nd} = -30.4).

Supraglacial streams are very dilute in Hf and Nd, precluding the measurement of Hf isotopes (Table 1). Neodymium isotopes in these waters are more radiogenic than the rivers and yield values of -34.6 and -32.4. In contrast, the lake sample is characterized by unradiogenic isotope compositions of -42.3 in Nd and of -15.7 in Hf, respectively.

4.3. Mineral abundances

Estimates of mineral abundances in the analysed rocks and a catchment sediment sample (JM1 – termed Sed 3 here) have been reported previously (Hindshaw et al., 2014). Applying the same methods (see section 3.5), two additional sediment samples - Soil 1 and PGL 2 - were analysed in this study in order to further constrain mineral compositions of sediments and potential variations (Table 3).

Sed 3 is a fine sand collected from the riverbank at the Leverett River water sampling location (location 1, Fig. 1b), similar to Sed 1 and 2 in Hindshaw et al. (2014) in terms of origin and grain-size. Soil 1 is finer grained and was collected beneath a few cm thick layer of soil with a grassy cover, north of the Leverett River sampling location (location 2, Fig. 1b). PGL 2 comes from the near shore ground of the same proglacial lake as PGL 1 of Hindshaw et al. (2014 - location 3, Fig. 1b). Overall, these three samples are very similar in their mineralogical composition (Table 3). Plagioclase (40 – 45 vol.%), quartz (34 to 38 vol.%), K-feldspar (8 – 17 vol.%) and minor biotite are largely derived from gneisses similar to Ro4 and possibly the Archean granite (see Fig. 4b in Hindshaw et al., 2014). Plagioclase, quartz and K-feldspar jointly comprise > 84 vol.% of the minerals. The occurrence of garnet (1.5 – 2.6 vol.%)

and hornblende (5.9 - 9.5%), as well as Ca-rich plagioclase, points to a small contribution from garnet amphibolites. Hornblende is only present at accessory levels in the characterized gneisses, contrasting with abundances of 45% and 68% in the amphibolites. Observed accessory minerals in sediments include clino- and orthopyroxene, biotite, titanite, epidote, magnetite, ilmenite, apatite and zircon.

The grey gneiss sample Ro4 has been reanalysed by point-counting here in order to better constrain its accessory mineral content and to obtain an estimate of a zircon free weathering endmember (section 5.5.2). Apatite abundance corresponds to ~ 0.15 vol.%, titanite to ~ 0.13 vol.% and zircon to ~ 0.02 vol.%. The corresponding wt.% are ~ 0.17, ~ 0.17 and ~ 0.034. The analysis revealed that epidote and chlorite show strong abundance variations. While the initial analysis gave an estimate of 1 vol.% chlorite and 7 vol.% epidote (Hindshaw et al., 2014), an estimate over six times the initial area, corresponding to 500 mm^2, yields 6 vol.% chlorite and 2 vol.% epidote. Epidote - which also occurs as veins - and mostly chlorite replace primary biotite and minute amounts of hornblende. Element maps show the existence of epidote (~ 80 %) and epidote-allanite (~ 20 %) with < 5 wt.% REE deduced from EMP analyses. Similarly, REE-poor and REE-rich phosphates are observed possibly resulting from metamorphic depletion of primary apatite minerals (Harlov et al., 2002).

For elemental and isotope budgets (sections 5.3 - 5.5) mineral weight percent is more useful than modal abundance. The density of catchment sediments is ~ 2.7 g/cm^3 based on mineral abundances, which is used for the conversion. Table 3 also lists weight percent ranges for minerals in sediments.

4.4. Hafnium and samarium/neodymium isotope systematics in sediments, rocks and mineral separates

4.4.1 Concentrations

Hafnium and neodymium concentrations are homogenous in hotplate digests of suspended load, spanning a range of 1.3-2.7 and 29.3-33.9 ppm, respectively (Table 2, Fig. 5). Catchment sediments from the proglacial area of Leverett are

more heterogeneous (mostly in the range of 2.4-7.5 ppm for Hf and 16.2-25.5 ppm for Nd) as are the bulk rocks (Hf: 0.7-3.7 ppm; Nd: 5.1-27.3 ppm). Among the catchment sediments Sed 1 is peculiar, with distinctly high concentrations in Hf and Nd (10.4 and 40.3 ppm, respectively). Hafnium concentrations measured in hotplate digests are between 42% and 91% of those obtained on fused powders. The implications of these differences in Hf concentrations are further discussed in section 5.5.2.

Mineral separates rich in Nd include titanite (772 and 1110 ppm), apatite (636 ppm) and to a lesser degree epidote, zircon, chlorite and hornblende (yielding up to 17.3-99.4 ppm, Table 2, Fig. 5). Hafnium is mostly contained in zircon separates (> 9000 ppm) and is also distinctly high in titanite (16.5 and 46.4 ppm). All further non-feldspar mineral separates - hornblende, garnet, clinopyroxene, epidote, chlorite - yield Hf concentrations between 0.3 and 3.2 ppm. Feldspar separates are low in Hf and Nd ranging between 0.05 and 0.65 ppm and 0.2 and 2.6 ppm, respectively.

In most cases, concentrations observed in single sedimentary mineral grains obtained by LA-ICP-MS overlap with the range observed in mineral separates (Fig. 5, Appendix S1). Hafnium in feldspar separates (0.05 to 1.5 ppm) is, however, somewhat higher than in measured sediment grains (mostly < 0.05 ppm). An analogous statement holds true for Nd in K-feldspar, where Nd amounts to 2.6 ppm in the separate and is < 0.2 ppm in single grains. These discrepancies possibly reflect, at least in part, the impact of inclusions in feldspars, which raise observed concentrations to higher values for mineral separates.

Samarium/neodymium and Hf/Nd ratios of sedimentary grains also overlap with mineral separates (Fig. 5, Appendix S1). Furthermore, Sm/Nd ratios suggest that sedimentary plagioclase is largely derived from gneisses whereas hornblende is sourced from mafic rocks, consistent with the previous notion based on mineral abundances in bulk rocks and plagioclase chemistry (section 4.3; Hindshaw et al., 2014).

Biotite (Hf < 0.05 ppm, Nd < 1.5 ppm), orthopyroxene (Hf < 0.06 ppm, Nd < 0.6 ppm), ilmenite (Hf < 0.9 ppm, Nd < 0.2 ppm) and oxides (Hf, Nd < 0.05 ppm) are depleted in REE and Hf (Appendix S1) and only occur as accessory

minerals. Hence, these minerals are irrelevant for elemental budgets in rivers and sediments and will not be considered further in the discussion. Apatite, on the other hand, is rich in REE and could affect sedimentary and riverine dissolved Nd budgets, and potentially dissolved Hf isotope compositions (Bayon et al., 2006).

4.4.2 Isotopes

Neodymium isotopes and Sm/Nd ratios in suspended load and catchment sediments are confined to the range between the grey (Ro4, ε_{Nd}= -39) and the pink orthogneiss (Ro2, ε_{Nd} = -31.4, Table 2, Fig. 4a). The suspended load is virtually constant in ε_{Nd} (-36.8 to -35.7) and on average ~3 units more radiogenic than Ro4. Catchment sediments are mostly between -34.2 and -33.3, but also include one sample with a signature similar to Ro4 and the rivers (MH1, -38.3). Hafnium isotopes show the least radiogenic values in felsic bulk rocks (ε_{Hf} = -59.9 to -55.1), and are progressively more radiogenic in catchment sediments (-54.4 to -47) and the suspended load (-46.4 to -34.6). The latter is offset from the dissolved load by at least ~20 ε_{Hf} (Fig. 4b). The two amphibolites (Ro1, Ro3) are very distinct in Nd-Hf isotope space, yielding ε_{Hf} > +26 and ε_{Nd} > -6.7, respectively.

The four rock samples Ro1 to Ro4 yield ages for the Sm/Nd isotope system ranging between 1746 and 1887 Myr, consistent with the literature (Table 4, Henriksen et al., 2000). With the exception of Ro1, the errorchrons are, however, characterized by mean square weighted deviations ≥ 140. Analysed mafic rocks and constituent minerals have Sm/Nd ratios ≥ 0.267 and are shifted towards more radiogenic ε_{Nd} at a given Sm/Nd ratio, resulting in higher initial $^{143}Nd/^{144}Nd$ ratios for their isochrons (Fig. 4a, Table 4). The garnet separates from PGL 2 are also characterized by high Sm/Nd ratios, but appear to be genetically linked to the gneisses rather than the sampled amphibolites (Fig. 4a). High Sm/Nd ratios and radiogenic Nd are also observed for titanite and hornblende within the gneisses, and in chlorite and epidote of Ro4. The measured Archean granite is less radiogenic than all other samples, yielding an ε_{Nd} of -47.3.

Consistent with the bulk rock Hf isotope compositions, mineral separates from the amphibolites are typically more radiogenic than those from the gneisses. Radiogenic Hf isotope compositions are, however, observed in gneissic titanite, epidote and hornblende (Table 2, Fig. 4b). The most notable minerals for the Hf systematics are the zircons in the gneisses – unradiogenic and with high Hf concentrations – and the extremely radiogenic garnets and apatites, yielding ε_{Hf} between +872 and +1940.

5. Discussion

5.1. Potential for external sources of hafnium and rare earth elements in rivers and streams

In principle, a significant fraction of the Hf and REEs in the sampled waters could be derived from external sources, rather than from weathering within the catchment. Precipitation as well as snow and ice-melt are insignificant sources of Hf and Nd, yielding a maximum contribution of 0.03% and 0.01% for the sampled lake. The calculation assumes element/Cl^- ratios similar to surface seawater of the neighbouring Labrador Sea (Filippova et al., 2017) and precipitation as the only source of Cl^- in the catchment (e.g., Yde et al., 2014)

Another potentially important external source is wind-blown dust from outside the catchment (Tepe and Bau, 2015). The samples likely to be affected most by external dust are the supraglacial streams, where any deposited dust might be less diluted compared to the sub- and proglacial area. Neodymium isotopes in two supraglacial streams are about 5 ε-units more radiogenic than the glacial samples (Table 1). This could imply addition of some external Nd to the catchment, but could also reflect a specific mineral assemblage exposed to weathering on the glacier resulting from sorting by wind *within* the catchment. Mineral sources of radiogenic Nd are abundant in the catchment rendering this interpretation entirely plausible (Fig. 4a).

Nevertheless, a small impact on dissolved isotopes in supraglacial streams due to partial dissolution of external dust cannot be precluded. Any impact on Leverett river waters is, however, unlikely since they are more concentrated in Hf and Nd than supraglacial streams by at least a factor of 69 and 116, respectively (Table 1). A potential source of REEs in Western Greenland is

Asian dust (Tepe and Bau, 2015). The more radiogenic signatures in supraglacial streams could be accounted for by ~ 15 % Nd from such dust, assuming a corresponding average Nd isotope composition of ~ -6 (Zhao et al., 2014). A similar dust-derived Nd contribution to the Leverett River would correspond to a Nd fraction < 0.12 %, and would imply a true weathering signal that is only marginally less radiogenic, by < 0.04 ε_{Nd}. Furthermore, the observed dissolved isotope compositions are entirely consistent with sampled rocks and sediments being the sole sources of dissolved Nd and Hf and no external sources are implied in any of the observations (section 5.3 - 5.5).

5.2. Carbonate versus silicate weathering

Solutes in glacial and non-glacial waters could reflect different mineralogical sources because the weathering process beneath the GRIS is different from the proglacial area in many respects, including water-rock interaction time, regolith/soil exposure age and access to atmospheric oxygen (Yde et al., 2010; Wimpenny et al., 2011; Hindshaw et al., 2014; Scribner et al., 2015). Although the weathered rocks are likely very similar, the different conditions may induce differences in mineral weathering reactions. For example, glacial activity could lead to continuous supply of trace carbonates from the bedrock, resulting in larger carbonate weathering contributions for glacial waters (e.g., Anderson et al., 2000). Hafnium/calcium ratios in Leverett River samples exceed 3×10^{-7} (Table 1), and are about two orders of magnitude higher than in the leached carbonate fraction of natural carbonate rocks (~ 7×10^{-9}, Rickli et al., 2013). These dissolved ratios are most likely much lower than the weathering released Hf/Ca ratios as a result of stronger adsorption of Hf onto suspended load. The observed variations in Hf isotopes between glacial and non-glacial waters, as well as temporal changes in Leverett River, therefore reflect changes in the weathering of different silicate minerals.

5.3. Hafnium and neodymium in sediments

The major element composition of catchment sediments and their plagioclase grains suggests large contributions from grey relative to pink orthogneisses and amphibolites (Hindshaw et al., 2014). The catchment sediments can,

hence, be modelled as Ro4 complemented with additional minerals like garnet and hornblende at their observed abundance in sediments (Table 3).

Catchment sediment Nd isotope compositions are consistent with 10 wt.% hornblende and 0.25 wt.% titanite added to Ro4, whereas the same additions scaled by a factor of 0.55 yield compositions similar to the suspended load (Fig. 6a). Titanite enrichments in catchment sediments relative to Ro4 are supported by elevated Ti concentrations (Hindshaw et al., 2014). Smaller effects in Nd isotope compositions are also modelled for garnet (~ 0.4 ε_{Nd} for 4 wt.%) and apatite (~ 1 ε_{Nd} for 0.2 wt.%) addition. There is, however, no evidence for apatite enrichment in sediments relative to Ro4.

In terms of the Nd budget, the modelled addition of titanite and hornblende to Ro4 produces a Nd concentration of about 29 ppm, versus observed values in catchment sediments that are mostly between 16.2 and 25.5 ppm (Table 2). Higher Nd concentrations are, however, observed in the suspended load (29.3-33.9 ppm, Table 2). The catchment sediments are probably depleted in REE-rich accessory minerals like allanite and monazite relative to the suspended load and Ro4, likely as a result of prevailing small sizes of these mineral grains (e.g., Garzanti et al., 2008).

As mentioned earlier, Hf isotope compositions in sediments cover a nearly continuous range, from ε_{Hf} = -54.4 in Sed 2 to -34.6 in a river suspended load sample (GR5, Fig 4b). Titanite and hornblende enrichment in sediments also shifts Hf isotope compositions to more radiogenic values compared to Ro4 (Fig. 6b, solid black line). The shift is, however, not sufficient to explain the Hf systematics: suspended load usually falls above the mixing line between Ro4 and titanite/hornblende in ε_{Hf} versus ε_{Nd} space, whereas catchment sediments are less radiogenic. The deviations from the mixing line can be reproduced by variable additions of zircon and garnet (Fig. 6b), using observed Hf concentrations as an additional constraint on zircon abundances (Fig. 6c). The calculations suggest that Hf isotopic variability in catchment sediments reflects variable abundances of garnet, ranging between ~ 1.1 and ~ 4 wt.%, coupled to variable zircon abundances of ~ 0.06 - 0.7 wt.‰ in excess of Ro4. The large range of Hf concentrations in catchment sediments, between 10.4 and 2.4 ppm, is controlled by zircon. Isotopic variations, however, also relate to variable

garnet abundances. A mixing calculation that only involves variation in amounts of zircon (Fig. 6c, grey dashed line) produces a larger range in Hf isotope compositions than observed. It should be noted that the Hf concentrations used in this modelling relate to those accessible in hotplate digestions, so that they represent a fraction of the constituent zircon (see section 5.5.2).

For river suspended loads a mixing model consistent with the isotope and concentration data is presented in Fig. 6b and c. Lower Hf concentrations in some of the suspended sediments imply a lower abundance of zircon than in Ro4. This is accounted for by including removal of zircons to model these observations, reflected by the negative signs in zircon ranges (Fig. 6b and c).

5.4. Sources of REE in rivers and streams

Dissolved Nd in glacial river samples is isotopically very similar to the grey orthogneiss Ro4 (Table 1, 2; Fig. 4a). This observation suggests that that the Nd isotope budget of glacial rivers is likely dominated by the nearly congruent dissolution of such gneisses. Clearly less radiogenic Nd isotope compositions than in Ro4 are, however, observed in the lake and two proglacial streams (Fig. 6d). Accessory minerals rich in REE, such as allanite and monazite, are probably more represented in these samples. In support of this interpretation, a missing unradiogenic Nd pool is implied in the Nd isotope composition of the bulk Ro4 relative to the measured minerals, with an approximate Nd isotope composition of -45.6 (Table 2). Selective weathering of unradiogenic Nd has been observed previously on glacially produced sediments, although the mineralogical source was not identified (Andersson et al., 2001).

Another possible source of unradiogenic Nd are Archean granites (ε_{Nd} = -47.3). However, if such granites were an important source of dissolved Nd, one would expect a clear shift towards less radiogenic Nd in Quinnguata Kuusua, given that it flows across the intrusion (GR7, Fig. 1). Rather, its Nd isotope composition of -39 is similar to samples from Akuliarusiarsuup Kuua and the Leverett River, which argues against Archean granites as a significant lithology controlling dissolved Nd isotope compositions. The Nd isotope composition of Quinnguata Kuusua is apparently acquired in the subglacial environment and

the interaction with the intrusion is too short to affect the dissolved composition.

5.5. Sources of hafnium in rivers and streams

The significance of a mineral for the dissolved Hf in rivers and streams will depend on its abundance, its Hf concentration and its susceptibility to weathering. In a simple illustrative case a mineral is abundant, rich in Hf and dissolving easily and will, hence, yield a large contribution to the dissolved Hf. The isotopic impact of a mineral also depends on the isotopic contrast relative to other minerals. Minerals with high Lu/Hf ratios, such as apatite and garnet, have highly radiogenic isotope signatures, so that even small contributions from their dissolution will substantially affect the dissolved Hf signatures.

In sections 5.5.3 and 5.5.4, we identify the sources of Hf in solution from isotope systematics in ε_{Hf} versus ε_{Nd} space and compare them with expectations from dissolution rates, given the observed mineral abundances, elemental concentrations and isotope compositions. But before doing so, we discuss the potential relevance of mineral inclusions (5.5.1) and the implications of a zircon free Ro4 for dissolved Hf isotope compositions (5.5.2).

5.5.1 Mineral inclusions

Observed mineral inclusions include apatite in clinopyroxene, hornblende and plagioclase, as well as quartz and clinopyroxene in garnet. Most likely, there are further minerals present as inclusions not mentioned here. The mineral digests could, hence, have a certain bias towards these inclusions, such that the mass balance calculations could be affected and misleading to some degree. The effect is expected to be small for two reasons: (1) estimates of mineral abundances also include observed mineral inclusions so that there should be no underestimation of accessory minerals such as apatite; (2) the key minerals used in the calculations show consistent isotope and concentration systematics where several measurements are available - garnets, zircons, titanite, hornblende (Table 2) – and are also consistent with the literature for apatite (e.g., Barford et al., 2004).

Feldspars separates are likely biased by inclusions since all separates yield higher concentrations than observed on single mineral grains by LA-ICP-MS (Table 2, Appendix S1). The weathering of these inclusions is likely to be strongly coupled to the weathering of the host, as the inclusions are typically only a few micrometres. Hence, it is justified to use the measured concentrations and isotope compositions of these separates, although the derived Hf and Nd will not reflect feldspar weathering in a strict sense. Measured feldspar isotope compositions are not extreme, so that a strong bias from mineral inclusions can be precluded (Table 2).

The model calculations use average concentrations and isotope compositions for separates of the same mineral – 5 for garnets, 2 for hornblende, titanite and zircon – also increasing their robustness. Note that, for hornblende, only the values for those in amphibolites are used (Ro1 and Ro3), because they are represented in the sediment (section 4.3).

5.5.2 Estimate of a zircon-free weathering endmember

The incongruency in Hf isotope weathering is thought to reflect a combination of the retention of unradiogenic Hf in zircons and the preferential weathering of high Lu/Hf phases (e.g., Bayon et al., 2006; Godfrey et al., 2007; Chen et al., 2013a). A constraint on the Hf isotope composition of a model zircon-free weathering endmember in the studied catchment is therefore valuable to compare the relative magnitude of these two phenomena. A large fraction of the Hf in the studied rocks and catchment sediments is accessed through hotplate digestion (42%-90%, Table 2), compared, for instance, to a fraction of 1.1% in young gneisses from the Swiss Alps (Verzasca catchment, Rickli et al., 2013). This means that zircons are easy to digest in the studied catchment, probably as a result of their age and the accumulated fission damage. Hotplate digests thus do not reflect the zircon-free Hf isotope compositions. Instead, an estimate of the zircon free Ro4 is derived from observed mineral abundances using two different but not fully independent mass balance considerations (see Appendix S3). The best estimate of this zircon free endmember yields a Hf concentration of 0.18 ppm and an ε_{Hf} of -5. Extreme estimates correspond to 0.17 ppm / -1.2 ε_{Hf} and 0.22 ppm / -16 ε_{Hf} , respectively. It could be argued

from these data alone that the glacial rivers result from the relatively congruent dissolution of the zircon free Ro4 only, but this is not a plausible interpretation given the large effect of garnet on dissolved riverine ε_{Hf} (section 5.5.3).

The estimate of the zircon free Hf concentration in Ro4 conflicts with models that explain the seawater array in terms of a consistent partitioning of Hf between zircons versus other upper crustal minerals. These models suggest that only ~65% of the Hf is zircon-bound (Chen et al., 2011; van de Flierdt, 2007), whereas it seems to be ~ 95% in Ro4 and ~ 99% in the Verzasca catchment (Rickli et al., 2013). The underlying model assumptions, namely that there is a close correspondence between Hf isotopes released by continental weathering and the seawater array (van de Flierdt et al., 2007) or a constant incongruent weathering effect in ε_{Hf} at any given ε_{Nd} (Chen et al., 2011), are not well constrained to date. Although this may be the case on a continental scale, it is certainly not the case for small catchments, which yield highly variable riverine ε_{Hf} at near constant ε_{Nd} (compare for instance data in Bayon et al., 2006; Godfrey et al., 2007 and Rickli et al., 2013).

5.5.3 Sources of dissolved hafnium from isotope systematics

To start with, we note that the relevance of allanite and monazite for dissolved Hf isotopes is not fully constrained since no mineral separates were measured for their Hf isotope compositions and concentrations. The mineral abundance of allanite is unlikely to exceed ~ 0.12 wt.% based on REE concentrations in sediments, assuming Nd concentrations of ~ 21'000 ppm as measured in a sedimentary allanite grain (Appendix S1) in the range of literature data (e.g, Gromet and Silver, 1983; Boston et al., 2017). Monazite abundance could be at most ~0.025 wt.% assuming Nd concentrations of 10 wt.%. Given typical Hf concentration in allanite < 0.7 ppm and in monazite < 1 ppm (Rubatto et al., 2006; Boston et al., 2017), allanite may yield an effect on dissolved Hf similar to apatite, which is discussed below. Monazite, on the other hand, can hardly be significant for dissolved Hf signatures.

Insights can be gained into the relative significance of apatite, titanite, garnet and hornblende as sources of radiogenic Hf in solution if they are added

to a model accessory mineral-free Ro4. The corresponding Hf concentration and isotope composition is estimated from feldspar, chlorite and epidote abundances in Ro4 and yields a value of ε_{Hf} = -38 and 0.15 ppm Hf. The corresponding Nd isotope composition, representing the same minerals and the REE-rich accessory minerals allanite and monazite, can also be derived from mass balance (ε_{Nd} = -42.7, Nd = 24.3 ppm).

At the observed abundance, not taking into account individual mineral weathering rates (see section 5.5.4), hornblende, garnet, titanite and apatite contribute significantly to radiogenic Hf isotopes in solution (Fig. 6d, dashed black lines). The influence on dissolved signatures decreases from garnet to titanite, hornblende and apatite. Combining only apatite, titanite and hornblende with the accessory mineral free Ro4 produces a trajectory, which yields Hf and Nd isotope compositions similar to glacial waters, although slightly too radiogenic in ε_{Hf} and ε_{Nd} (Fig. 6d, solid black line). The possibility that the slightly different ε_{Nd} is due to low dissolution rates of horblende is discussed later (section 5.5.4). The offset in ε_{Hf} is unexpectedly low, since garnets are common in the catchment and should have a significant impact on all water samples. Some zircon likely compensates for garnet weathering: Adding 2 wt.% garnet and 1/500 of this amount of zircon to the mixing trajectory at the Nd isotope composition of Ro4 (black circle) yields Hf isotope composition in the range of glacial waters. Similarly, non-glacial streams can be modelled by a combination of 3 wt.% garnet and 1/10'000 this amount of zircon, or 2.5 wt% garnet and no zircon (Fig. 6d, lines with arrows).

The model does not claim that only zircon can compensate for radiogenic Hf from garnet. However, the zircon-derived amount of Hf in the model that reproduces glacial waters is 0.4 ppm. This is nearly three times the Hf concentration of the accessory mineral free Ro4. Hence, most of the compensation must be accomplished by zircon.

Two further findings should be mentioned here. Firstly, very efficient subglacial weathering of zircon, meaning that most of the hotplate digestion accessible Hf is released, can be precluded since radiogenic accessory minerals could not compensate for this process. A complete dissolution of the measured Ro4 would imply unrealistic garnet contributions of ~10 wt.% to explain

glacial samples (Fig. 6d, grey dashed line). Secondly, it also seems unlikely that hornblende, titanite or apatite are strongly overrepresented in the dissolved load as this would result in more radiogenic dissolved Nd isotope compositions than observed (Fig. 6d).

5.5.4 Mineral weathering rates

Mineral weathering reactions are confined to mineral surfaces (e.g., Brantley and Olsen, 2014). As a result dissolution rates scale with surface area and small minerals will contribute much to the weathering flux. In the subglacial environment all minerals are likely abundant in the fine fraction as a result of glacial grinding. Hence, differences in dissolution rates relating to surface area are reduced. This could be different in non-glacial streams since much of the weathered substrate can be relatively coarse. Larger garnet contributions in these streams could therefore reflect small grain sizes of garnet relative to other minerals in the proglacial zone, but this is not consistent with observed garnet sizes in catchment sediments.

Figure 7 shows laboratory based surface area-normalised dissolution rates as a function of pH for many relevant minerals in the catchment (Guidry and Mackenzie, 2003; Palandri and Kharaka, 2004 and references therein). Conditions correspond to 25°C and solutions far from mineral saturation. At the neutral to alkaline pH relevant to the sampled waters (Table 1, pH = 6.8 – 9.3) apatite dissolution rates are similar to, but slightly faster than, the dissolution of almandine garnet. Titanite dissolution is probably similar to garnet (see Morton, 1984; Bateman and Catt, 1985). Laboratory based dissolution rates observed for hornblende are variable (Sverdrup, 1990; Frogner and Schweda, 1998; Golubev et al., 2005). In field studies hornblende appears to be relatively stable (Colman, 1982), so that the lower laboratory-based rates are possibly more representative. The dissolution rates for garnet, apatite and titanite, hence, suggest that the relative abundances of these minerals should be reflected in dissolved Hf as their dissolution rates are relatively similar at neutral to alkaline pH. Hornblende, on the other hand, may be underrepresented relative to apatite, titanite and garnet. At conditions close to mineral saturation, dissolution rates decrease (e.g., Brantley and Olsen,

2014), which provides an explanation for the different Hf isotope compositions in glacial and non-glacial waters as discussed below (section 5.6.1.).

5.6. Controls on dissolved hafnium isotopes

The two most striking features regarding dissolved Hf isotope compositions are the large variations at the beginning of the Leverett time series (Fig. 2) and the large isotopic contrast between glacial and non-glacial samples (Fig. 4). Previous work on radiogenic Sr and Pb has highlighted two key aspects, which can affect the congruency in released isotopes relative to weathered source rocks, namely regolith exposure age (e.g., Blum and Erel, 1997; Bullen et al., 1997; Harlavan et al., 1998), and water-rock interaction time (Bullen et al., 1996; Hindshaw et al., 2014; Arendt et al, 2016). The data obtained in this study provide some insights into the significance of water-rock interaction time (5.6.1) and regolith exposure (5.6.2) for the release of Hf isotopes, given the constraints on landscape exposure to weathering from moraine ages (Fig. 1).

5.6.1. Water-rock interaction time

Water-rock interaction times are very variable for waters discussed here. Subglacial water in distributed systems can interact with sediments for more than half a year, from the cessation of the channelized system in August/September until the next melting season (Chu et al., 2016). These waters can yield high dissolved concentrations (Graly et al., 2014) and, likely, saturation with respect to reactive minerals. The influence of less reactive minerals will therefore increase, since they will continue to dissolve. In contrast, fresh melt in summer will only take up to 4 days to reach the outlet of the Leverett Glacier from inland moulins (Chandler et al., 2013). Similar time spans will also apply for the rock-interaction time of non-glacial streams before they join the large glacial rivers.

The first two dissolved Hf isotope compositions of Leveret River were obtained during the final meltwater pulse event of the 2009 season, during which seven surface lakes drained and expelled long-term stored subglacial meltwater from the bed of the ice sheet (Fig. 2a, Bartholomew et al., 2011).

This caused up-glacier expansion of the fast/efficient channelized system at the expense of a slow/inefficient distributed drainage system. The flushing of basal waters, which have interacted with the subglacial sediment for an extended period of time, is consistent with the enrichment of the bulk runoff in solutes and elevated electrical conductivity, starting with the water pulse and ending at around the 9th of July (Fig. 2b, e.g., Cuffey and Paterson, 2010; Bhatia et al., 2011; Hindshaw et al.; 2014). Such waters, which do not reflect very recent melt, are referred to as delayed waters (e.g., Bhatia et al., 2011). The unradiogenic Hf isotope composition of the first two samples, therefore, reflects higher proportions of delayed waters compared to later sampling occasions, when recent glacial melt draining to the bed through crevasses, moulins and englacial channels increasingly constituted the water flux of the river. The large contrast between the first two observations, whereby the second seems more influenced by delayed waters than the first, may imply isolated water reservoirs with heterogeneous ε_{Hf} compositions beneath the glacier, reservoirs that are accessed gradually by the extending channelized draining system.

The clear difference in Hf isotope compositions between glacial and non-glacial waters probably also results from different average water-rock interaction times. The channelized drainage system beneath the Leverett Glacier expands inland over the course of the melting season (Bartholomew et al., 2010; Chandler et al., 2013), which implies a continuous source of delayed waters (e.g., Bhatia et al., 2011; Chandler et al., 2013). In contrast, the Hf isotopic composition of non-glacial streams results from the short timescale interaction of these waters with the rock and regolith substrate, as they flow in the shallow zone above the permafrost horizon. More radiogenic Hf isotope compositions in non-glacial compared to glacial waters are thus an expression of their short water-rock interaction time, whereby the released Hf isotope signal is more influenced by weathering of reactive and radiogenic minerals, especially garnet. Glacial waters, on the other hand, are more controlled by weathering of unradiogenic and less reactive minerals, in particular zircon (Fig. 6d). The strong contrast in Hf concentrations of supraglacial melt (0.06 to 0.2 pmol/l) and the Leverett River (13.9 to 42.7 pmol/l; Table 2) also suggests that

the Hf isotope composition of delayed waters will exert a strong control on the bulk isotope composition of the river.

5.6.2. Regolith exposure age

It could be argued that the availability of freshly ground and strained mineral surfaces, produced continuously through the active sliding of warm-based glaciers (Cuffey and Paterson, 2010), results in a bias towards unradiogenic Hf from zircons (Piotrowski et al., 2000; van de Flierdt et al., 2002). Non-glacial streams, on the other hand, would potentially lack this source as strained surfaces anneal over time in the proglacial area. Two arguments can be made against this interpretation. In a detailed study of Sr isotopes at Leverett Glacier in July 2009, Hindshaw et al. (2014) documented a clear change in Sr isotope composition at the transition from a distributed to a channelized subglacial drainage system. Although a mobile element like Sr, which is abundant in a range of minerals with variable weathering susceptibility, could be more prone to respond to water-rock interaction time, it seems unlikely that the underlying processes for Sr and Hf isotopes are completely different. In addition, the lake sample measured in this study is most likely strongly influenced by weathering of long-exposed proglacial material, as it is situated west of the Ørkendalen moraines, which are 6.8 kyrs old (Levy et al., 2012). Nevertheless, the lake yields a Hf isotope composition similar to glacial samples (Fig. 6d), probably as a result of the long residence time of water in the lake (c.f., Anderson et al., 2001). Although, high Cl^- concentrations in streams indicate that non-glacial streams are fed by lakes, their Hf isotope composition is much more radiogenic. This probably reflects removal of Hf from lakes, possibly through adsorption onto diatoms (Stichel et al., 2012a) and an overprint of Hf isotope signatures in streams. In support of this interpretation, Si concentrations are very low in the lake (Table 1) and diatoms constitute some of the deposited sediment (Willemse, 2002).

5.7 Implications

The new observations clearly show that glacial weathering processes increase the congruency in Hf isotope weathering compared to the glacial forefield. Such

a direct influence of ice-sheets on the release of Hf isotopes was previously only inferred indirectly from observations in marine ferromanganese precipitates (Gutjahr et al., 2014; Piotrowski et al., 2000; van de Flierdt et al., 2002). The more congruent Hf signals in glacially sourced waters compared to the non-glacial streams support the interpretation that more crustal-like ε_{Hf} in the North Western Atlantic since ~3 Ma relates to the onset of northern hemispheric glaciation (van de Flierdt et al., 2002). The glacial rivers studied here are, however, not distinctly unradiogenic in Hf in general terms, since they fall close to the seawater array in Hf-Nd isotope space (Fig. 4b).

For the studied area, extended water-rock interaction time in subglaical settings is likely more relevant for the release of unradiogenic Hf than the effect of glacial grinding (section 5.6). A strong influence of strained zircon surfaces on dissolved Hf isotopes also seems inconsistent with observations on a longer time scale (Gutjahr et al., 2014). If the availability of freshly ground rock substrate was crucial for the release of unradiogenic Hf, it would probably lead to a co-evolution of ε_{Hf} and Pb isotopes in seawater during the deglacial since both isotope systems would be governed by the exposure and weathering of glacial material and a short oceanic residence time (20 to 30 yr for Pb in the Atlantic, Henderson and Maier-Reimer, 2002). While efficient zircon weathering would gradually decrease in the newly forming glacial forefields - reflecting zircon annealing - weathering of newly exposed allanite, apatite and titanite with radiogenic Pb and Hf isotopes (Harlavan et al., 1998; Harlavan and Erel, 2002; Bayon et al., 2006), would be expected to intensify. Recent observations indicate, however, a ~5 kyr earlier change towards more radiogenic Hf in the Northwest Atlantic after the last glacial maximum than is observed for Pb isotopes (Gutjahr et al., 2014). Although seawater Pb isotope evolution is governed by the exposure of radiogenic minerals in Pb in glacial forefields (Harlavan et al., 1998; Foster and Vance, 2006), Hf isotopes appear to be mostly responsive to changes in subglacial hydrology (this study, Gutjahr et al., 2014). This does not preclude the release of highly radiogenic Hf during the weathering of glacially produced sediments: The non-glacial streams studied here are very radiogenic, which supports the notion that glacially sourced

sediments could be the cause for radiogenic Hf isotopes in the Kalix River (Chen et al., 2013b).

In general, currently available dissolved Hf and Nd isotopes of rivers do not reproduce seawater compositions, which are characterized by relatively homogenous ε_{Hf} in the open ocean and a relatively systematic relationship with ε_{Nd} (Godfrey et al., 2009; Rickli et al., 2009; 2010; 2014; Zimmermann 2009a; Stichel et al., 2012a,b). Larger variability in ε_{Hf} is observed in semi-enclosed basins like the Baltic and the Labrador Sea (Chen et al., 2013b; Filippova et al., 2017). Riverine Hf isotope compositions are, in contrast to the open ocean, highly variable at a given Nd isotope composition (c.f., this study; Bayon et al., 2006; Godfrey et al., 2007; Zimmermann et al., 2009b; Chen et al., 2013b; Rickli et al., 2013). The discordance between seawater Hf-Nd isotope compositions and rivers is unexpected given recent estimates of the seawater residence time of Hf (Chen et al., 2013b; Filippova et al., 2017), which is most likely shorter than that of Nd (< 500 yr, Siddall et al., 2008). This could suggest that a further significant source of Hf in seawater is more homogeneous than rivers, possibly representing an exchange process at the ocean boundary as observed for Nd (Lacan and Jeandel, 2005). Clay sized sediments are indeed rather homogenous in ε_{Hf} (Bayon et al., 2016) implying that the release of Hf from fine sediments deposited in the ocean could be the sought-after source (Albarède et al., 1998). Alternatively, unradiogenic riverine fluxes in Hf may be balanced by radiogenic fluxes on a larger scale, leading to overall homogenous riverine inputs to the oceans. If that turns out to be the case, it would justify models that interpret the seawater array as a result of a consistent partitioning of Hf between zircon and other minerals in the upper continental crust (van de Flierdt et al., 2007; Chen et al., 2011) and a constant effect of incongruent weathering for the zircon free crust on large scales (Chen et al., 2011). It would also support the idea, that the "clay array" mostly reflects weathering released Hf (Bayon et al., 2016), without any significant contributions of Hf from primary minerals including zircon.

6. Conclusions

This study represents the first comprehensive attempt to understand the hydrological and mineralogical factors that affect and control the release of Hf isotopes into the hydrosphere in a high latitude setting characterized by glacial activity. To this end, we have measured Hf and Nd isotopes and concentrations in catchment rocks, corresponding mineral separates, catchment sediments, riverine suspended load as well as glacially fed rivers and non-glacial streams. These analyses are complemented by the mineralogical characterization of sediment samples from the catchment, providing an estimate of the mineralogy of weathered material.

Hafnium and neodymium isotope compositions of catchment sediments and riverine suspended load are well reconciled with the measured Hf and Nd isotope compositions and concentration in bulk rocks and mineral separates. Specifically, their Nd isotope composition is consistent with a typical gneissic composition in the catchment, slightly enriched in titanite and including amphibolite derived hornblende. The Hf isotopic range in sediments additionally requires variable proportions of highly radiogenic garnets and variable trace amounts of unradiogenic zircon.

Dissolved Hf and Nd isotopes in waters show very different characteristics. Neodymium isotopes closely mirror the isotope composition of representative gneisses in the catchment (ε_{Nd} = -39) and cover a small range in all glacially fed and non-glacial waters (ε_{Nd} = -42.8 to -37.9). Dissolved Hf isotopes, on the other hand, are shifted to much more radiogenic values than bulk gneisses (ε_{Hf} = -55.1) yielding values close to the seawater array for glacial rivers (ε_{Hf} = -18.3 to -0.9) and between +15.8 and +46.3 for non-glacial streams.

Two hypotheses can explain the strong contrast in dissolved Hf isotopes in glacial and non-glacial waters. First, it could imply a larger influence of zircon weathering in glacial rivers due to the availability of glacially strained zircon surfaces. Second, it could reflect different average water-rock interaction times and, as a result, different contributions from reactive/radiogenic versus weathering resistant/unradiogenic minerals. Glacial rivers receive continuous contributions from long interacting waters of distributed subglacial drainage systems, whereas non-glacial streams are characterized by fast superficial drainage above the permafrost horizon. The implied short interaction time

increases the significance of garnet over zircon weathering, mostly as a result of the chemical inertness of zircons relative to garnet. Although it may be premature to draw a firm conclusion as to which process is more dominant, the current observations favour water-rock interaction time. The sampled lake, for instance, is chemically closely related to non-glacial streams, yet shows a Hf isotope signature in the range of glacial rivers, probably due to the long water residence time in the lake. Similarly, increasingly warmer ice sheets produced less congruent weathering in Hf isotopes in the early stages of the last deglaciation (Gutjahr et al., 2014), probably due to more efficient subglacial drainage and a shortening of water-rock interaction times.

Acknowledgements

We thank the Bristol Isotope Group and Chris Coath for their support in the beginning of this study. Corey Archer, Manuela Fehr and Colin Maden are thanked for running and maintaining the isotope labs in Zurich during the finalization of this work. Thomas Kokfelt and his colleagues at the Geological Survey of Denmark and Greenland kindly provided the Archean granite sample. Irene Ivanov-Bucher (ETH Zurich) initially separated minerals for the project and generously separated more garnets in 2016. Giuditta Fellin (ETH Zurich) kindly separated apatites. We thank three anonymous reviewers, and the associate editor for their comprehensive and valuable comments. The study was supported by the Swiss National Foundation and the European Commission (SNF fellowship 127764, Marie-Curie Fellowship Project No. 253117 to JR). The field season in 2006 was funded by NERC (grant no. NE/B502701/1) and the one in 2009 by EPSRC (grant no. EP/D057620) and NERC (grant no. NE/G00496X/1).

References

Albarède F., Simonetti A., Vervoort J.D., Blichert-Toft J. and Abouchami W. (1998) A Hf-Nd isotopic correlation in ferromanganese nodules. *Geophys. Res. Lett.* **25**, 3895-3898.

Anderson N.J., Harriman R., Ryves D.B. and Patrick S.T. (2001) Dominant factors controlling variability in the ionic composition of West Greenland Lakes. *Arct. Antarct. Alp. Res.* **33**, 418-425.

Anderson S.P. (2007) Biogeochemistry of glacial landscape systems. *Annu. Rev. Earth Planet. Sci.* **35**, 375-399.

Anderson S.P., Derver J.I. and Humphrey N.F. (1997) Chemical weathering in glacial environments. *Geology* **25**, 399-402.

Anderson S.P., Drever J.I., Frost C.D. and Holden P. (2000) Chemical weathering in the foreland of a retreating glacier. *Geochim. Cosmochim. Acta* **64**, 1173-1189.

Andersson P.S., Dahlqvist R., Ingri J. and Gustafsson O. (2001) The isotopic composition of Nd in a boreal river: A reflection of selective weathering and colloidal transport. *Geochim. Cosmochim. Acta* **65**, 521-527.

Arendt C.A., Stevenson E.I. and Aciego S.M. (2016) Hydrologic controls on radiogenic Sr in meltwater from an alpine glacier system: Athabasca Glacier, Canada. *Appl. Geochem.* **69**, 42-49.

Barfod G.H., Krogstad E.J., Frei R. and Albarède F. (2005) Lu-Hf and PbSL geochronology of apatites from Proterozoic terranes: A first look at Lu-Hf isotopic closure in metamorphic apatite. *Geochim. Cosmochim. Acta* **69**, 1847-1859.

Bartholomew I., Nienow P., Mair D., Hubbard A., King M.A. and Sole A. (2010) Seasonal evolution of subglacial drainage and acceleration in a Greenland outlet glacier. *Nat. Geosci.* **3**, 408-411.

Bartholomew I., Nienow P., Sole A., Mair D., Cowton T., Palmer S. and Wadham J. (2011) Supraglacial forcing of subglacial drainage in the ablation zone of the Greenland ice sheet. *Geophys. Res. Lett.* **38**.

Bateman R.M. and Catt J.A. (1985) Modification of heavy mineral assemblages in English coversands by acid pedochchemical weathering. *Catena* **12**, 1-21.

Bayon G., Dennielou B., Etoubleau J., Ponzevera E., Toucanne S. and Bermell S. (2012) Intensifying weathering and land use in iron age Central Africa. Science **335**, 1219-1222.

Bayon G., Skonieczny C., Delvigne C., Toucanne S., Bermell S., Ponzevera E. and André L. (2016) Environmental Hf-Nd isotopic decoupling in World river clays. *Earth Planet. Sci. Lett.* **438**, 25-36.

Bayon G., Vigier N., Burton K.W., Brenot A., Carignan J., Etoubleau J. and Chu N.C. (2006) The control of weathering processes on riverine and seawater hafnium isotope ratios. *Geology* **34**, 433-436.

Bhatia M.P., Das S.B., Kujawinski E.B., Henderson P., Burke A. and Charette M.A. (2011) Seasonal evolution of water contributions to discharge from a Greenland outlet glacier: insight from a new isotope-mixing model. *J. Glaciol.* **57**, 929-941.

Blum J.D. and Erel Y. (1997) Rb/Sr isotope systematics of a granitic soil chronosequence: The importance of biotite weathering. *Geochim. Cosmochim. Acta* **61**, 3193-3204.

Boston K.R., Rubatto D., Hermann J., Engi M. and Amelin Y. (2017) Geochronology of accessory allanite and monazite in the Barrovian metamorphic sequence of the Central Alps, Switzerland. *Lithos* **286**, 502-518.

Brantley S.L. and Olsen A.A. (2014) 7.3 - Reaction Kinetics of Primary Rock-Forming Minerals under Ambient Conditions in: Holland, H.D., Turekian, K.K. (Eds.), Treatise on Geochemistry (Second Edition). Elsevier, Oxford, pp. 69-113.

Bullen T., White A., Blum A., Harden J. and Schulz M. (1997) Chemical weathering of a soil chronosequence on granitoid alluvium: II. Mineralogic and isotopic constraints on the behavior of strontium. *Geochim. Cosmochim. Acta* **61**, 291-306.

Bullen T.D., Krabbenhoft D.P. and Kendall C. (1996) Kinetic and mineralogic controls on the evolution of groundwater chemistry and 87Sr/86Sr in a sandy silicate aquifer, northern Wisconsin, USA. *Geochim. Cosmochim. Acta* **60**, 1807-1821.

Cappelen J., Jørgensen B.V., Laursen E.V., Stannius L.S. and Thomsen R.S. (2001) The observed climate of Greenland, 1958-99 – with climatological standard normals, 1961–90, Tech. Rep. 00- 18. Danish Meteorological Institute.

Chaïrat C., Schott J., Oelkers E.H., Lartigue J.E. and Harouiya N. (2007) Kinetics and mechanism of natural fluorapatite dissolution at 25 °C and pH from 3 to 12. *Geochim. Cosmochim. Acta* **71**, 5901-5912.

Chandler D.M., Wadham J.L., Lis G.P., Cowton T., Sole A., Bartholomew I., Telling J., Nienow P., Bagshaw E.B., Mair D., Vinen S. and Hubbard A. (2013) Evolution of the subglacial drainage system beneath the Greenland Ice Sheet revealed by tracers. *Nat. Geosci.* **6**, 195-198.

Chen T.-Y., Ling H.-F., Frank M., Zhao K.-D. and Jiang S.-Y. (2011) Zircon effect alone insufficient to generate seawater Nd-Hf isotope relationships. *Geochem. Geophys.* **12**, QO5003, doi: 5010.1029/2010gc003363.

Chen T.Y., Frank M., Haley B.A., Gutjahr M. and Spielhagen R.F. (2012) Variations of North Atlantic inflow to the central Arctic Ocean over the last 14 million years inferred from hafnium and neodymium isotopes. *Earth Planet. Sci. Lett.* **353-354**, 82-92.

Chen T.Y., Li G.J., Frank M. and Ling H.F. (2013a) Hafnium isotope fractionation during continental weathering: Implications for the generation of the seawater Nd-Hf isotope relationships. *Geophys. Res. Lett.* **40**, 916-920.

Chen T.Y., Stumpf R., Frank M., Beldowski J. and Staubwasser M. (2013b) Contrasting geochemical cycling of hafnium and neodymium in the central Baltic Sea. *Geochim. Cosmochim. Acta* **123**, 166-180.

Chu W., Schroeder D.M., Seroussi H., Creyts T.T., Palmer S.J. and Bell R.E. (2016) Extensive winter subglacial water storage beneath the Greenland Ice Sheet. *Geophys. Res. Lett.* **43**, 12,484-412,492.

Colman S.M. (1982) Chemical Weathering of Basalts and Andesites: Evidence from Weathering Rinds. *U.S. Geol. Surv. Prof. Pap.* **1246**, 51 pp.

Cuffey K.M. and Paterson W.S.B. (2010) The Physics of Glaciers, Fourth Edition. Academic Press

Dausmann V., Frank M., Gutjahr M. and Rickli J. (2017) Glacial reduction of AMOC strength and long-term transition in weathering inputs into the Southern Ocean since the mid-Miocene: Evidence from radiogenic Nd and Hf isotopes. *Paleoceanography* **32**, 265-283.

Dausmann V., Frank M., Siebert C., Christl M. and Hein J.R. (2015) The evolution of climatically driven weathering inputs into the western Arctic Ocean since the late Miocene: Radiogenic isotope evidence. *Earth Planet. Sci. Lett.* **419**, 111-124.

David K., Frank M., O'Nions R.K., Belshaw N.S. and Arden J.W. (2001) The Hf isotope composition of global seawater and the evolution of Hf isotopes in the deep Pacific Ocean from Fe-Mn crusts. *Chem. Geol.* **178**, 23-42.

Escher A., Sørensen K. and Zeck H.P. (1976) Nagssugtoqidian mobile belt in West Greenland, in: Escher, A., Watt, W.S. (Eds.), Geology of Greenland. Grønlands Geologiske Undersøgelse.

Filippova A., Frank M., Kienast M., Rickli J., Hathorne E., Yashayaev I.M. and Pahnke K. Water mass circulation and weathering inputs in the Labrador Sea based on coupled Hf-Nd isotope compositions and rare earth element distributions. *Geochim. Cosmochim. Acta*.

Filippova A., Frank M., Kienast M., Rickli J., Hathorne E., Yashayaev I.M. and Pahnke K. (2017) Water mass circulation and weathering inputs in the Labrador Sea based on coupled Hf–Nd isotope compositions and rare earth element distributions. *Geochim. Cosmochim. Acta* **199**, 164-184.

Frogner P. and Schweda P. (1998) Hornblende dissolution kinetics at 25 degrees C. *Chem. Geol.* **151**, 169-179.

Gaillardet J., Dupré B., Louvat P. and Allègre C.J. (1999) Global silicate weathering and CO2 consumption rates deduced from the chemistry of large rivers. *Chem. Geol.* **159**, 3-30.

Garzanti E., Andò S. and Vezzoli G. (2008) Settling equivalence of detrital minerals and grain-size dependence of sediment composition. *Earth Planet. Sci. Lett.* **273**, 138-151.

Godfrey L.V., King R.L., Zimmermann B., Vervoort J.D. and Halliday A. (2007) Extreme Hf isotope signals from basement weathering and its influence on the seawater Hf-Nd isotope array. *Geochim. Cosmochim. Acta* **71**, A334-A334.

Godfrey L.V., Zimmermann B., Lee D.C., King R.L., Vervoort J.D., Sherrell R.M. and Halliday A.N. (2009) Hafnium and neodymium isotope variations in NE Atlantic seawater. *Geochem. Geophys.* **10**, Q08015, doi: 08010.01029/02009gc002508.

Golubev S.V., Pokrovsky O.S. and Schott J. (2005) Experimental determination of the effect of dissolved CO2 on the dissolution kinetics of Mg and Ca silicates at 25 degrees C. *Chem. Geol.* **217**, 227-238.

Graly J.A., Humphrey N.F., Landowski C.M. and Harper J.T. (2014) Chemical weathering under the Greenland ice sheet. *Geology* **42**, 551-554.

Gromet L.P. and Silver L.T. (1983) Rare-Earth Element Distributions among Minerals in a Granodiorite and Their Petrogenetic Implications. *Geochim. Cosmochim. Acta* **47**, 925-939.

Guidry M.W. and Mackenzie F.T. (2003) Experimental study of igneous and sedimentary apatite dissolution: Control of pH, distance from equilibrium, and temperature on dissolution rates. *Geochim. Cosmochim. Acta* **67**, 2949-2963.

Guillong M., Meier D.L., Allan M.M., Heinrich C.A. and Yardley B.W.D. (2008) SILLS: A matlab-based programm for the reduction of Laser Ablation ICP-MS data of homogenous materials and inclusions. *Mineralogical Association of Canada Short Course 40*, 328-333.

Gutjahr M., Frank M., Lippold J. and Halliday A.N. (2014) Peak Last Glacial weathering intensity on the North American continent recorded by the authigenic Hf isotope composition of North Atlantic deep-sea sediments. *Quat. Sci. Rev.* **99**, 97-117.

Harlavan Y. and Erel Y. (2002) The release of Pb and REE from granitoids by the dissolution of accessory phases. *Geochim. Cosmochim. Acta* **66**, 837-848.

Harlavan Y., Erel Y. and Blum J.D. (1998) Systematic Changes in Lead Isotopic Composition with Soil Age in Glacial Granitic Terrains. *Geochim. Cosmochim. Acta* **62**, 33-46.

Harlov D.E., Andersson U.B., Förster H.J., Nyström J.O., Dulski P. and Broman C. (2002) Apatite-monazite relations in the Kiirunavaara magnetite-apatite ore, Northern Sweden. *Chem. Geol.* **191**, 47-72.

Hasholt B. and Sogaard H. (1978) Et forsøg pa en klimatisk– hydrologisk regionsinddeling af Holsteinsborg kommune (Sisimut). *Geografisk Tidsskrift* **77**, 72-92.

Henderson G.M. and Maier-Reimer E. (2002) Advection and removal of 210Pb and stable Pb isotopes in the oceans: A general circulation model study. *Geochim. Cosmochim. Acta* **66**, 257-272.

Henriksen N., Higgins A.K., Kalsbeek F. and Pulvertaft T.C.R. (2000) Greenland from Archaean to Quaternary: descriptive text to the geological map of Greenland, 1:2 500 000. *Geol. Greenland Sur. Bull.* **185**.

Hindshaw R.S., Rickli J., Leuthold J., Wadham J. and Bourdon B. (2014) Identifying weathering sources and processes in an outlet glacier of the Greenland Ice Sheet using Ca and Sr isotope ratios. *Geochim. Cosmochim. Acta* **145**, 50-71.

Jochum K.P., Weis U., Stoll B., Kuzmin D., Yang Q., Raczek I., Jacob D.E., Stracke A., Birbaum K., Frick D.A., Günther D. and Enzweiler J. (2011a) Determination of Reference Values for NIST SRM 610–617 Glasses Following ISO Guidelines. *Geostand. Geoanal. Res.* **35**, 397-429.

Jochum K.P., Wilson S.A., Abouchami W., Amini M., Chmeleff J., Eisenhauer A., Hegner E., Iaccheri L.M., Kieffer B., Krause J., McDonough W.F., Mertz-Kraus R., Raczek I., Rudnick R.L., Scholz D., Steinhoefel G., Stoll B., Stracke A., Tonarini S., Weis D., Weis U. and Woodhead J.D. (2011b) GSD-1G and MPI-DING Reference Glasses for In Situ and Bulk Isotopic Determination. *Geostand. Geoanal. Res.* **35**, 193-226.

Levy L.B., Kelly M.A., Howley J.A. and Virginia R.A. (2012) Age of the Orkendalen moraines, Kangerlussuaq, Greenland: constraints on the extent of the southwestern margin of the Greenland Ice Sheet during the Holocene. *Quat. Sci. Rev.* **52**, 1-5.

Ludwig, K.-R. (2012) User's manual for isoplot 3.75. A geochronological toolkit for Microsoft Excel. Berkeley Geochronology Center Special Publication **No.5**, 1–75.

Ma J., Wei G., Xu Y. and Long W. (2010) Variations of Sr–Nd–Hf isotopic systematics in basalt during intensive weathering. *Chem. Geol.* **269**, 376-385.

Meierbachtol T., Harper J. and Humphrey N. (2013) Basal Drainage System Response to Increasing Surface Melt on the Greenland Ice Sheet. *Science* **341**, 777-779.

Merschel G., Bau M., Schmidt K., Münker C. and Dantas E.L. (2017, in press) Hafnium and neodymium isotopes and REY distribution in the truly dissolved, nanoparticulate/colloidal and suspended loads of rivers in the Amazon Basin, Brazil. *Geochim. Cosmochim. Acta*., doi.org/10.1016/j.gca.2017.07.006

Morton A.C. (1984) Stability of detrital heavy minerals in tertiary sandstones from the North-Sea Basin. *Clay Minerals* **19**, 287-308.

Münker C., Weyer S., Scherer E. and Mezger K. (2001) Separation of high field strength elements (Nb, Ta, Zr, Hf) and Lu from rock samples for MC-ICPMS measurements. *Geochem. Geophys.* **2**, doi:10.1029/2001GC000183.

Nowell G.M., Kempton P.D., Noble S.R., Fitton J.G., Saunders A.D., Mahoney J.J. and Taylor R.N. (1998) High precision Hf isotope measurements of MORB and OIB by thermal ionisation mass spectrometry: insights into the depleted mantle. *Chem. Geol.* **149**, 211-233.

Palandri J.L. and Kharaka Y.K. (2004) A compilation of rate parameters of water-mineral interaction kinetics for application for geochemical modeling. *U.S.G.S., Open File Report 2004-1068*.

Palmer S., Shepherd A., Nienow P. and Joughin I. (2011) Seasonal speedup of the Greenland Ice Sheet linked to routing of surface water. *Earth Planet. Sci. Lett.* **302**, 423-428.

Patchett P.J. and Tatsumoto M. (1980) A Routine High-Precision Method for Lu-Hf Isotope Geochemistry and Chronology. *Contrib. Mineral. Petrol.* **75**, 263-267.

Patchett P.J., White W.M., Feldmann H., Kielinczuk S. and Hofmann A.W. (1984) Hafnium/rare earth element fractionation in the sedimentary system and crustal recycling into the Earth's mantle. *Earth Planet. Sci. Lett.* **69**, 365-378.

Pin C. and Zalduegui J.F.S. (1997) Sequential separation of light rare-earth elements, thorium and uranium by miniaturized extraction chromatography: Application to isotopic analyses of silicate rocks. *Anal. Chim. Acta* **339**, 79-89.

Piotrowski A.M., Lee D.C., Christensen J.N., Burton K.W., Halliday A.N., Hein J.R. and Günther D. (2000) Changes in erosion and ocean circulation recorded in the Hf isotopic compositions of North Atlantic and Indian Ocean ferromanganese crusts. *Earth Planet. Sci. Lett.* **181**, 315-325.

Rickli J., Frank M., Baker A.R., Aciego S., de Souza G., Georg R.B. and Halliday A.N. (2010) Hafnium and neodymium isotopes in surface waters of the eastern Atlantic Ocean: Implications for sources and inputs of trace metals to the ocean. *Geochim. Cosmochim. Acta* **74**, 540-557.

Rickli J., Frank M. and Halliday A.N. (2009) The hafnium-neodymium isotopic composition of Atlantic seawater. *Earth Planet. Sci. Lett.* **280**, 118-127.

Rickli J., Frank M., Stichel T., Georg R.B., Vance D. and Halliday A.N. (2013) Controls on the incongruent release of hafnium during weathering of metamorphic and sedimentary catchments. *Geochim. Cosmochim. Acta* **101**, 263-284.

Rickli J., Gutjahr M., Vance D., Fischer-Gödde M., Hillenbrand C.-D. and Kuhn G. (2014) Neodymium and hafnium boundary contributions to seawater along the West Antarctic continental margin. *Earth Planet. Sci. Lett.* **394**, 99-110.

Rubatto D., Hermann J. and Buick I.S. (2006) Temperature and Bulk Composition Control on the Growth of Monazite and Zircon During Low-pressure Anatexis (Mount Stafford, Central Australia). *J. Petrol.* **47**, 1973-1996.

Scholz H. and Baumann M. (1997) An 'open system pingo' near Kangerlussuaq (Søndre Strømfjord), West Greenland. *Geol. Greenland Sur. Bull.* **176**, 104-108.

Siddall M., Khatiwala S., van de Flierdt T., Jones K., Goldstein S.L., Hemming S. and Anderson R.F. (2008) Towards explaining the Nd paradox using reversible scavenging in an ocean general circulation model. *Earth Planet. Sci. Lett.* **274**, 448-461.

Stichel T., Frank M., Rickli J. and Haley B.A. (2012a) The hafnium and neodymium isotope composition of seawater in the Atlantic sector of the Southern Ocean. *Earth Planet. Sci. Lett.* **317**, 282-294.

Stichel T., Frank M., Rickli J.r., Hathorne E.C., Haley B.A., Jeandel C. and Pradoux C. (2012b) Sources and input mechanisms of hafnium and neodymium in surface waters of the Atlantic sector of the Southern Ocean. *Geochim. Cosmochim. Acta* **94**, 22-37.

Sverdrup H.U. (1990) The Kinetics of Base Cation Release due to Chemical Weathering. Lund University Press, Lund.

Tatenhove F.G.M.V. (1996) Changes in morphology at the margin of the Greenland ice sheet (Leverett Glacier), in the period 1943–1992: a quantitative analysis. *Earth Surf. Processes Landforms* **21**, 797-816.

Taylor A. and Blum J.D. (1995) Relation between soil age and silicate weathering rates determined from the chemical evolution of a glacial chronosequence. *Geology* **23**, 979-982.

Tepe N. and Bau M. (2015) Distribution of rare earth elements and other high field strength elements in glacial meltwaters and sediments from the western Greenland Ice Sheet: Evidence for different sources of particles and nanoparticles. *Chem. Geol.* **412**, 59-68.

Thirlwall M.F. (1991) Long-term reproducibility of multicollector Sr and Nd isotope ratio analysis. *Chem. Geol.* **94**, 85-104.

van de Flierdt T., Frank M., Lee D.C. and Halliday A.N. (2002) Glacial weathering and the hafnium isotope composition of seawater. *Earth Planet. Sci. Lett.* **201**, 639-647.

Vance D. and Thirlwall M. (2002) An assessment of mass discrimination in MC-ICPMS using Nd isotopes. *Chem. Geol.* **185**, 227-240.

Vervoort J.D., Plank T. and Prytulak J. (2011) The Hf-Nd isotopic composition of marine sediments. *Geochim. Cosmochim. Acta* **75**, 5903-5926.

Willemse N. (2002) Holocene sedimentation history of the shallow Kangerlussuaq lakes, West Greenland, Meddelelser om Gronland. *Meddelelser om Grønland* **41**, 1-48.

Wimpenny J., Burton K.W., James R.H., Gannoun A., Mokadem F. and Gislason S.R. (2011) The behaviour of magnesium and its isotopes during glacial weathering in an ancient shield terrain in West Greenland. *Earth Planet. Sci. Lett.* **304**, 260-269.

Wimpenny J., James R.H., Burton K.W., Gannoun A., Mokadem F. and Gislason S.R. (2010) Glacial effects on weathering processes: New insights from the elemental and lithium isotopic composition of West Greenland rivers. *Earth Planet. Sci. Lett.* **290**, 427-437.

Yde J.C., Knudsen N.T., Hasholt B. and Mikkelsen A.B. (2014) Meltwater chemistry and solute export from a Greenland Ice Sheet catchment, Watson River, West Greenland. *J. Hydrol.* **519**, 2165-2179.

Zhao W.C., Sun Y.B., Balsam W., Lu H.Y., Liu L.W., Chen J. and Ji J.F. (2014) Hf-Nd isotopic variability in mineral dust from Chinese and Mongolian deserts: implications for sources and dispersal. *Scientific Reports* **4**.

Captions

Table 1: Chemical and physical characteristics, as well as Nd and Hf isotopic compositions, of the sampled rivers, streams and the lake. pH, T, Ca, Mg, Na, K, Si, $HCO3^-$, SO_4^{2-}, Cl^- and TSS have been compiled from the literature, where the exact coordinates of sampling locations can also be found (Hindshaw et al., 2014; Wimpenny et al., 2010; 2011). External errors on isotope ratios are discussed in section 3.4.

Table 2: Elemental concentrations (Hf, Sm, Nd) and isotope compositions (Hf, Nd) of bulk rocks, minerals, catchment sediments and riverine suspended load. Hafnium concentrations for bulk rocks and catchment sediments are reported for hotplate digests (HP) and fused powders (see section 3.3). External errors on isotope ratios are discussed in section 3.4.

Table 3: Mineral abundances in rocks and sediments. Compositions of rocks Ro1 - Ro3 and Sed 3 are from Hindshaw et al. (2014). Ro4 has been reanalysed (see section 4.3).

Table 4: Ages for the four studied rocks based on the Sm/Nd isotope system. Ages were calculated using Isoplot (Ludwig, 2012).

Figure 1: (a) Water sampling sites and geology underlying the Kangerlussuaq region of Southwest Greenland, also including moraines (Levy et al., 2012 and references therein). The inlet shows the study area within Greenland. (b) Detailed map of the sampling locations on Leverett Glacier. (X) denotes the Lake, (Y) the sampled supraglaical stream. Catchment sediments are from the Lake (X), the sampling location on Leverett River (1) and to the north of it (2), a proglacial lake (3), the end moraine (4), dirt cones on Leverett Glacier (5), a proglacial stream (6) and northern and southern lateral moraines (7, 8). Topography and geomorphology are based on Scholz and Baumann (1997).

Figure 2: Leverett time series of (a) discharge, (b) electrical conductivity (EC), (c) Hf and Nd concentrations and (e, f) isotope compositions in July 2009. Discharge and conductivity data are from Bartholomew et al. (2011).

Figure 3: Composition of sampled waters in terms of major cations (a) and anions (b) in terms of molar abundances. (Data sources are given in the caption for Table 1).

Figure 4: Neodymium isotope composition vs molar Sm/Nd ratios for all water and solid samples (a). Hafnium vs neodymium isotope compositions are shown in (b) in the context of the terrestrial and the seawater array, including the defining data (small grey symbols, Albarède et al., 1998; David et al., 2001; Vervoort et al., 2011). Light blue symbols refer to the Leverett time series samples, dark blue ones to further glacial samples collected elsewhere (see Table 1).

Figure 5: Hafnium and neodymium concentrations in bulk rocks, mineral separates, catchment sediments and riverine suspended load (a, b), along with molar ratios of Sm/Nd and Hf/Nd for these and water samples (c, d). Grey circles show results for laser analysis of single mineral grains from a variety of catchment sediments (Appendix S1). Hafnium bulk sample concentrations of fused powders are not shown. The feldspar separate from Ro4 represents a mixture of K-feldspar and plagioclase.

Figure 6: Mixing models to evaluate key minerals affecting the Hf and Nd isotope compositions observed in the riverine dissolved load, suspended load and in catchment sediments. All mixing calculations use average compositions (Sm/Nd, ε_{Nd}, ε_{Hf}) for titanite, hornblende derived from amphibolites and garnets. (a) Sm/Nd systematics in catchment sediments, suspended load and river waters. Neodymium isotopes in catchment sediments are consistent with the addition of 0.25 wt.% titanite and 10 wt.% hornblende to Ro4. The Sm-Nd systematics of the suspended load is also consistent with the addition of such a titanite-hornblende mixture, though at a smaller contribution (55%) relative to the catchment sediments . Also shown is the individual impact of each mineral added to Ro4. (b) ε_{Hf} vs ε_{Nd} for suspended load and catchment sediments. The variation in ε_{Hf} is in agreement with variable amounts of garnet and zircon over

and above the variations resulting from titanite and hornblende (see panel a). Implied garnet abundances are consistent with observations in catchment sediments, while zircon abundances are constrained by observed Hf concentrations in catchment sediments and suspended load. (c) ε_{Hf} vs 1/Hf for all sediments and the fitted relationships for the mixtures illustrated in b. Modelled sedimentary compositions are in good agreement with the observations, for which a linear regression is shown (grey line, r^2=0.82, p <0.001). Larger variations in ε_{Hf} would result for catchment sediments if their Hf isotope compositions and concentrations only reflected variable zircon abundances at a constant garnet abundance (grey dashed line). (d) Mixing models for dissolved Hf. Mixtures of different minerals with the accessory mineral free Ro4 illustrate their significance for dissolved Hf isotopes. Adding titanite, hornblende and apatite to the accessory mineral free Ro4 defines the black solid trajectory, which, complemented by garnet and zircon, reproduces Hf in glacial and non-glacial waters (black arrows starting from the trajectory at an Ro4-like ε_{Nd}, black circle). Also shown is a mixture between the measured Ro4 and garnet (grey dashed line). Less radiogenic ε_{Nd} in some proglacial rivers and the lake likely reflect higher weathering contributions from allanite and monazite (section 5.4).

Figure 7: Surface-area normalised dissolution rates for minerals in the catchment. The rates are fitted to laboratory observations at 25°C far from mineral saturation (Guidry and Mackenzie, 2003; Palandri and Kharaka, 2004 and references therein). Hornblende data is from Sverdrup et al. (1990, green fitted line), Golubev et al. (2005, green circles) and Frogner and Schweda (1998, green diamonds). Apatite dissolution rates are nearly constant in a pH-range from 6 to 10 (Chaïrat et al., 2007), so that the fit given here by Guidry and Mackenzie (2003) can be extended to the pH range of the figure. Dissolution rates of oligoclase under basic conditions are not available and albite rates are plotted instead. The shaded area depicts the pH range of studied waters.

Sample	Type	Date	Time	pH	T	Ca	Mg	Na	K	Si	HCO_3^-	SO_4^{2-}	Cl^-	TDS	TSS	Hf	Sm	Nd	εHf	2 SEM	εNd	2 SEM
					°C	µmol/l									g/l	pmol/l				int		int
Regional sampling - 2006																						
GR10	fjord	-	-	6.96	10.5	615.0	2940.0	>2000	586.0	26.6	266.0	1890.0	42300.0	48623.6	-	-	-	-	-	-	-40.82	0.15
GR11	non-glacial	15.7.06	-	6.81	10.0	105.0	86.3	99.1	15.6	76.1	358.0	17.2	94.0	851.3	0.004	-	-	-	+17.9	0.3	-38.73	0.07
GR12	non-glacial	14.7.06	-	8.30	19.3	665.0	775.0	539.0	142.0	323.0	1740.0	263.0	596.0	5043.0	0.014	-	-	-	+15.8	0.2	-42.80	0.07
GR13	non-glacial	15.7.06	-	7.65	14.2	148.0	116.0	136.0	40.5	6.9	532.0	22.0	105.0	1106.4	-	-	-	-	+46.3	0.5	-39.61	0.08
GR14[a]	non-glacial	18.7.06	-	8.10	7.5	229.0	91.1	362.0	11.2	59.5	556.0	72.0	324.0	1704.8	-	-	-	-	+13.5	0.7	-30.40	0.07
GR15	non-glacial	16.7.06	-	8.25	12.3	181.0	202.0	171.0	82.7	4.2	784.0	28.4	119.0	1572.3	-	-	-	-	+43.3	1.4	-40.72	0.11
GR1	glacial	11.7.06	-	8.48	4.2	24.8	8.3	11.6	12.2	19.6	72.8	8.3	2.0	159.5	0.44	-	-	-	-7.2	0.3	-39.22	0.08
GR2	glacial	11.7.06	-	7.91	4.2	32.9	11.0	29.9	18.2	21.6	98.5	13.4	6.0	231.5	0.60	-	-	-	-12.2	0.2	-39.30	0.07
GR4	glacial	12.7.06	-	7.11	6.0	40.8	11.6	32.2	20.2	25.7	119.0	19.5	4.3	273.3	0.85	-	-	-	-13.7	0.3	-39.18	0.12
GR5	glacial	13.7.06	-	7.18	3.0	39.2	11.4	30.2	18.6	24.8	145.0	16.8	5.2	291.2	0.40	-	-	-	-13.6	0.2	-39.07	0.10
GR7	glacial	13.7.06	-	7.30	8.6	42.4	13.7	35.4	21.6	28.7	133.0	19.3	4.1	298.2	0.55	-	-	-	-14.7	0.8	-38.97	0.12
GR8	glacial	14.7.06	-	7.20	5.5	40.6	14.4	37.7	22.9	42.1	151.0	17.9	3.2	329.8	0.44	-	-	-	-0.9	0.6	-39.51	0.09
GR9	glacial	14.7.06	-	7.18	5.3	31.1	9.7	8.0	9.8	21.7	99.3	10.7	-	190.3	-	-	-	-	-6.6	0.4	-37.95	0.07
Leverett time series - 2009																						
Lev6	glacial	6.7.09	09:10	9.34	0.1	56.0	13.7	89.9	48.4	36.8	185.3	29.5	6.6	466.2	7.4	42.7	689.9	4984.5	-13.7	0.2	-38.62	0.08
Lev8	glacial	8.7.09	17:45	8.02	0.2	26.6	7.1	35.9	25.2	17.2	99.3	11.2	4.1	226.7	3.3	24.4	457.8	3310.6	-18.3	0.2	-38.35	0.07
Lev10	glacial	10.7.09	08:30	8.22	0.2	31.9	8.0	42.4	29.0	20.3	128.4	15.2	4.8	280.1	2.9	30.6	564.8	4065.9	-9.1	0.1	-38.49	0.09
Lev12	glacial	12.7.09	18:10	7.92	0.3	26.5	6.6	30.6	23.4	15.3	110.2	11.5	3.4	227.5	2.3	19.2	357.0	2585.3	-11.4	0.2	-38.63	0.06
Lev14	glacial	14.7.09	08:00	8.21	0.2	30.9	8.3	35.2	23.8	20.2	113.2	14.0	3.2	248.7	3.2	15.8	278.7	2017.1	-9.9	0.4	-38.41	0.07
Lev18	glacial	18.7.09	08:10	8.25	0.1	36.2	8.5	39.0	25.5	20.9	104.6	15.6	4.4	254.8	3.0	19.0	376.8	2651.3	-11.2	0.3	-38.51	0.07
Lev20	glacial	20.7.09	17:20	7.81	0.1	30.4	7.6	33.6	21.9	17.0	100.5	13.1	3.2	227.3	-	17.4	370.6	2666.2	-12.4	0.2	-38.54	0.09
Lev22	glacial	22.7.09	08:15	8.08	0.1	35.7	8.4	37.6	24.6	19.1	109.1	17.1	4.1	255.7	3.3	20.7	363.4	2611.0	-12.3	0.2	-38.29	0.08
Lev24	glacial	24.7.09	17:50	7.88	0.1	33.5	8.7	36.7	23.9	17.9	99.9	15.4	4.4	240.4	-	17.3	329.1	2386.6	-11.8	0.3	-38.43	0.08
Lev26	glacial	26.7.09	08:10	8.08	0.1	35.9	8.3	37.3	23.6	19.9	110.7	16.4	4.9	257.0	4.2	16.7	319.7	2305.7	-11.7	0.2	-38.52	0.07
Lev28	glacial	28.7.09	18:00	8.28	0.1	39.4	8.7	38.9	24.7	20.6	126.2	17.8	3.2	279.6	3.6	13.9	266.3	1909.2	-11.5	0.4	-38.40	0.09
CampLake	lake	17.7.09	16:00	8.93	14.0	834.0	1134.5	1008.5	400.1	0.0	3767.0	30.0	1099.0	8273.1	-	5.6	92.7	644.1	-15.7	0.5	-42.32	0.09
SGlacial23[b]	supraglacial	23.7.09	14:00	5.31	0.1	0.0	0.0	0.4	0.1	0.1	NA	0.0	0.2	0.8	-	0.06	2.0	12.1	-	-	-32.40	0.20
SGlacial29[b]	supraglacial	29.7.09	16:00												-	0.20	3.1	16.4	-	-	-34.56	0.11

[a] Sample from close to Sisimut

[b] Chemical composition reflects the average of two glacial samples from Hindshaw et al. (2014)

Table 1

	Hf ppm (HP)	Hf (fused)	Sm	Nd	εHf	2 SEM int	εNd	2 SEM int
Ro1 - Garnet Amphibolite	1.40	2.71	4.48	16.11	+26.4	0.2	-6.71	0.09
Garnet	0.63		1.39	4.04	+1308.3	0.3	+2.78	0.09
Hornblende	2.02		7.05	22.65	+1.6	0.3	-1.83	0.13
Plagioclase	0.28		0.39	1.27	-27.1	0.6	-2.71	0.13
Ro3 - Amphibolite	0.72	0.95	1.60	5.10	+27.3	0.4	+1.00	0.07
Clinopyroxene	0.73		0.41	1.12	-7.7	0.4	+8.29	0.15
Epidote	1.06		9.10	29.25	+122.8	0.5	+2.19	0.11
Hornblende	0.93		1.19	2.79	+8.5	0.4	+16.94	0.11
Plagioclase	0.05		0.23	0.67	+65.2	0.5	+6.22	0.28
Rutile	4.48		2.41	5.39	+39.2	0.5	+19.06	0.17
Ro2 - Orthogneiss	3.65	4.90	1.85	10.51	-59.9	0.2	-31.44	0.07
Chlorite	3.21		4.78	38.82	-59.8	0.3	-42.78	0.26
Epidote	2.18		15.59	99.42	-25.2	0.3	-30.44	0.07
K-feldspar	1.46		0.38	2.59	-61.4	0.1	-35.99	0.09
Plagioclase	0.66		0.05	0.24	-60.6	0.2	-29.82	0.16
Titanite	46.40		330.48	772.31	+20.9	0.1	+4.43	0.09
Zircon	10827.61		47.04	74.04	-61.4	0.1	-19.74	0.10
Ro4 - Orthogneiss	1.63	3.86	3.86	27.30	-55.1	0.2	-39.04	0.22
Chlorite	0.50		0.51	1.86	-50.3	0.7	-16.42	0.14
Epidote	1.73		14.17	34.53	-18.1	0.2	+2.11	0.14
Feldspar	0.08		0.04	0.22	-58.1	0.6	-33.03	0.15
Hornblende	2.23		8.67	33.35	-21.5	0.2	-17.63	0.12
Titanite	16.47		397.73	1109.51	+116.6	0.2	-5.34	0.13
Zircon	9130.48		5.88	18.90	-61.2	0.1	-32.13	0.20
Archean granite	0.97		2.01	19.99	-58.43	0.2	-47.33	0.06
Bulk catchment sediments [a]								
Sed 1 - river sediment	10.42	20.85	7.13	40.29	-53.1	0.1	-34.01	0.06
Sed 2 - river sediment	7.51	12.76	4.52	25.45	-54.4	0.1	-33.29	0.06
LC sand - river sand	2.59	5.09	2.96	17.06	-51.0	0.1	-33.79	0.08
SM Sed - side moraine	2.75	6.25	3.49	20.34	-47.0	0.1	-33.86	0.07
PGL 1 - proglacial lake	3.95	5.55	3.16	18.29	-52.4	0.2	-34.24	0.09
MH1 - dirt cone sediment	2.17	3.10	2.43	16.23	-53.0	0.2	-38.28	0.07
MH2 - dirt cone sediment	5.80	6.38	3.21	18.47	-53.2	0.1	-33.90	0.06
Garnet PGL 2								
Garnet a	0.49		2.44	5.38	+871.9	0.4	+7.42	0.08
Garnet b	0.46		2.78	6.66	+1247.4	0.4	+3.65	0.08
Garnet c	0.35		3.54	8.27	+1308.1	0.5	+3.72	0.06
Garnet d	0.26		2.90	5.73	+1940.2	0.5	+15.06	0.07
Apatite Sed 3, PGL 2	0.73		192.98	636.65	+1148.9	2.3	-16.33	0.09
Bulk riverine suspension								
Lev14	2.04		4.68	30.03	-43.3	0.3	-36.05	0.07
Lev18	2.16		4.65	29.36	-	-	-35.86	0.09
Lev20	2.28		4.86	30.67	-45.3	0.6	-35.78	0.08
Lev22	2.30		4.67	29.50	-45.3	0.6	-35.84	0.07
Lev24	2.72		4.77	30.00	-46.3	0.6	-35.81	0.08
Lev26	2.61		4.98	31.42	-46.4	0.5	-35.80	0.07
Lev28	1.92		4.63	29.33	-44.5	0.8	-35.96	0.09
GR1	1.39		5.26	33.89	-35.8	0.5	-35.74	0.11
GR2	1.59		5.15	32.27	-39.9	0.6	-35.85	0.07
GR4	1.42		4.68	29.90	-40.5	0.5	-36.81	0.09
GR5	1.46		4.65	30.01	-34.6	0.3	-36.83	0.07
GR8	1.26		5.16	33.31	-39.8	0.3	-36.43	0.09

[a] Some of the sediment labels in Table 2 of Hindshaw et al. (2014) were confounded. The correct labels for LC Sand, SM Sed, MH1 and PGL1 are SM Sed, PGL1, LC Sand and MH1. These misrepresentations have no effect on the discussions and conclusions in Hindshaw et al. (2014).

Table 2

	vol. %							wt.%
	Ro1	Ro3	Ro2	Ro4	Sed 3	Soil 1	PGL 2	in sediments
Major minerals								
Clinopyroxene		22			<1	<1	2.2	<2.8
Garnet	4				1.5	2.6	2.6	2.1-3.7
Hornblende	68	45		<1	5.9	8.6	9.5	7.2-11.7
Scapolite		12			-	-	-	-
K-feldspar			24	44	8.3	16.9	7.5	7.3-16.3
Plagioclase	14	18	50	21	42.0	40.4	45.5	38.8-44.1
Quartz	10		22	27	33.8	37.6	34.3	33-36.8
Accessory minerals								
Apatite			1	~ 0.15	<1	<1	<1	<1.2
Biotite					<1	1.3	1.2	<1.4
Chlorite			2	6	-	-	-	-
Epidote		3	<1	2	<1	-	<1	<1.3
Ilmenite			1		<1	<1	1.0	<1.7
Orthopyroxene					<1	<1	<1	<1.2
Magnetite	1				-	<1	<1	<1.9
Titanite	3	<1	<1	~ 0.13	<1	-	<1	<1.3
Zircon			<1	~ 0.02	<1	<1	<1	<1.7

Table 3

	Age (Myr)	Initial 143Nd/144Nd	Uncertainty (2σ)	MSWD
Ro1 - Garnet Amphibolite	1855 ± 87	0.51025	0.00011	2.7
Ro3 - Amphibolite	1746 ± 200	0.51053	0.00028	140
Ro2 - Orthogneiss	1776 ± 320	0.50984	0.00030	2436
Ro4 - Orthogneiss	1887 ± 230	0.50970	0.00028	384

Table 4

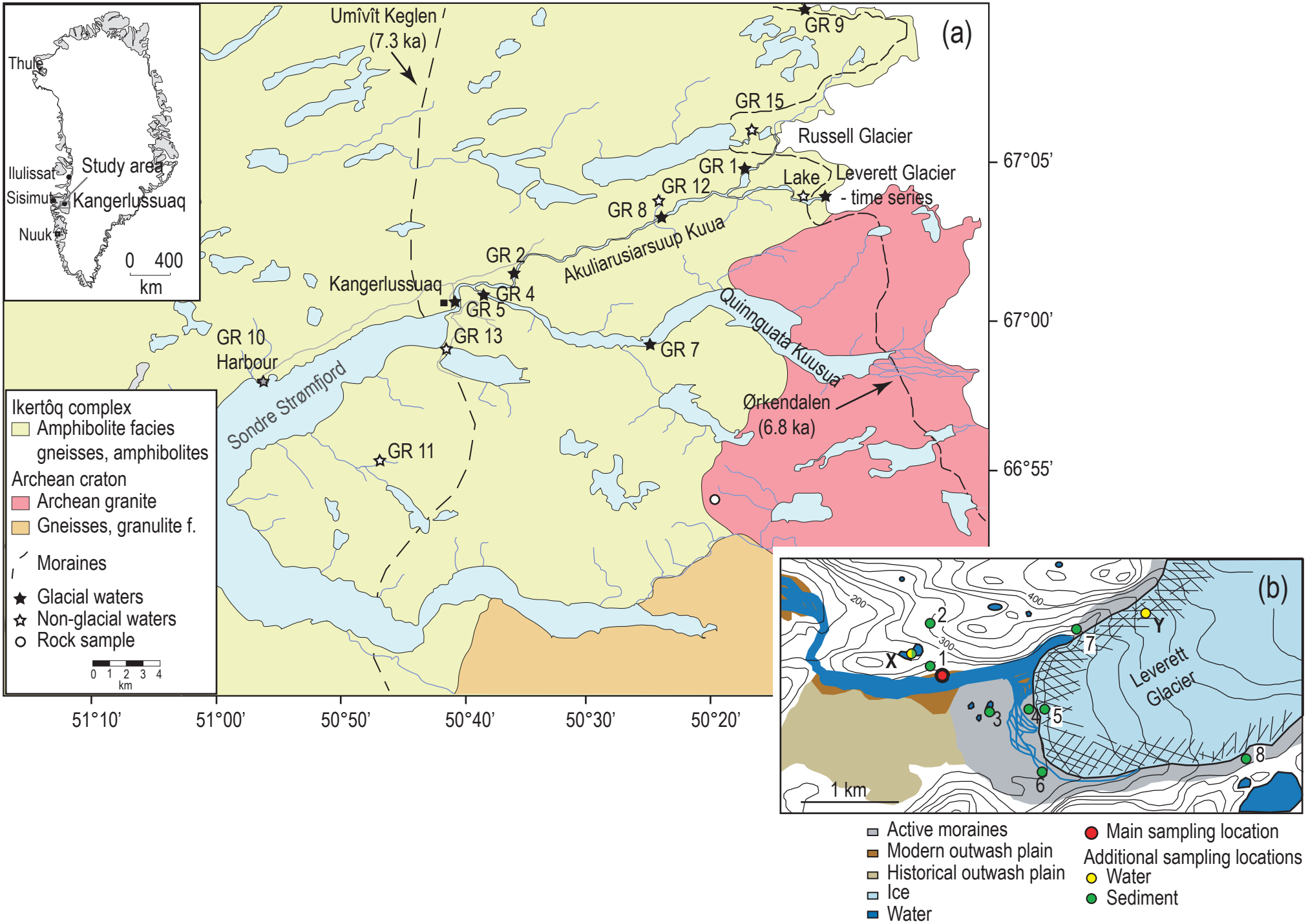
(a)
Thule
Ilulissat
Sisimiut
Study area
Kangerlussuaq
Nuuk
0 400
km
Umîvît Keglen
(7.3 ka)
GR 9
GR 15
Russell Glacier
GR 1
Lake
Leverett Glacier
- time series
GR 12
GR 8
Akuliarusiarsuup Kuua
GR 2
Kangerlussuaq
GR 4
GR 5
GR 13
GR 10
Harbour
Sondre Strømfjord
GR 7
Quinnguata Kuusua
Ørkendalen
(6.8 ka)
GR 11
67°05'
67°00'
66°55'
51°10'
51°00'
50°50'
50°40'
50°30'
50°20'
Ikertôq complex
Amphibolite facies
gneisses, amphibolites
Archean craton
Archean granite
Gneisses, granulite f.
Moraines
Glacial waters
Non-glacial waters
Rock sample
0 1 2 3 4
km
(b)
200
300
400
X
Y
1
2
3
4
5
6
7
8
Leverett
Glacier
1 km
Active moraines
Modern outwash plain
Historical outwash plain
Ice
Water
Main sampling location
Additional sampling locations
Water
Sediment

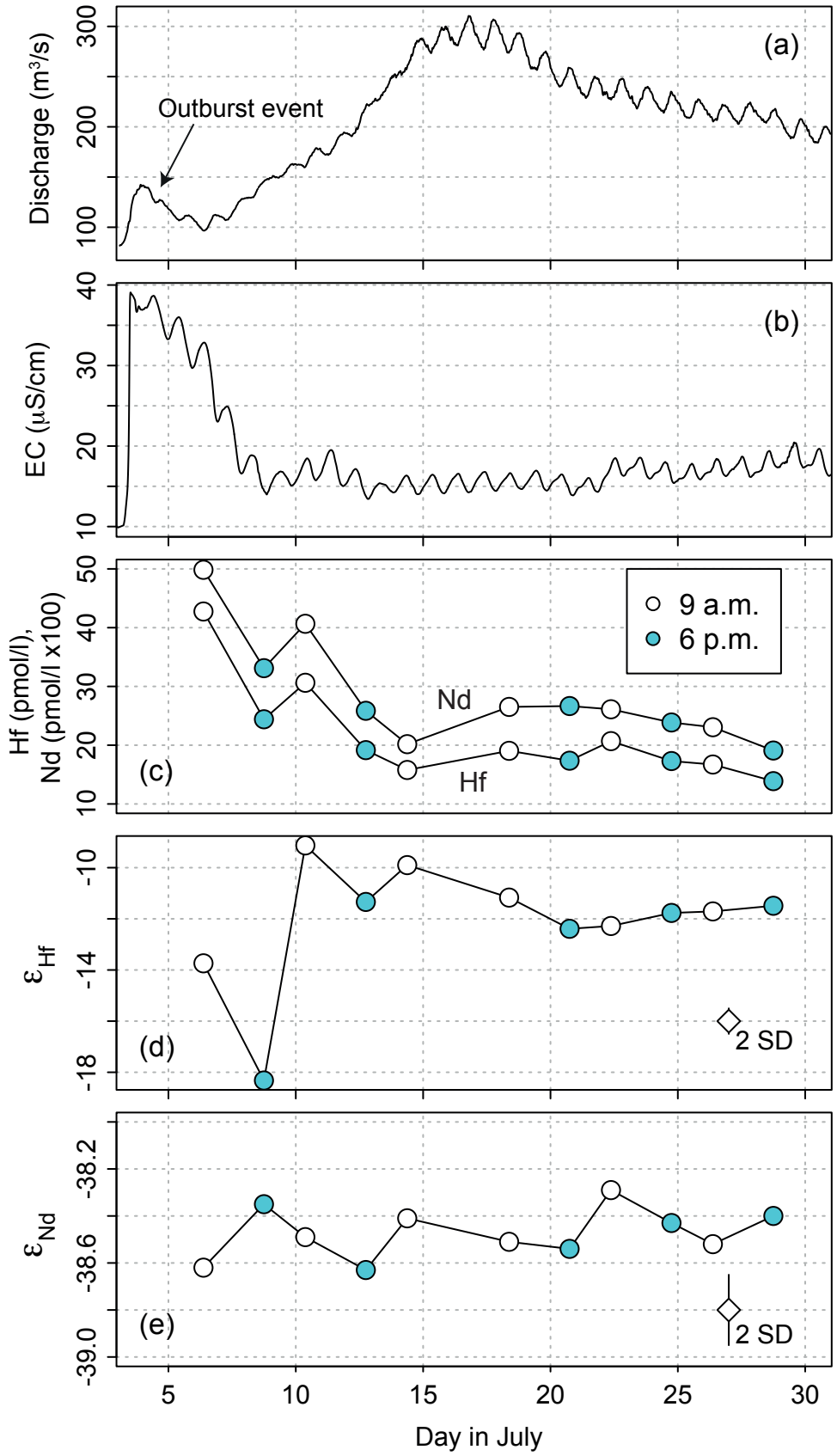
Discharge (m³/s)
300
200
100
(a)
Outburst event
EC (µS/cm)
40
30
20
10
(b)
Hf (pmol/l),
Nd (pmol/l x100)
50
40
30
20
10
9 a.m.
6 p.m.
Nd
Hf
(c)
ε_Hf
-10
-14
-18
(d)
2 SD
ε_Nd
-38.2
-38.6
-39.0
(e)
2 SD
5
10
15
20
25
30
Day in July

Fig. 2

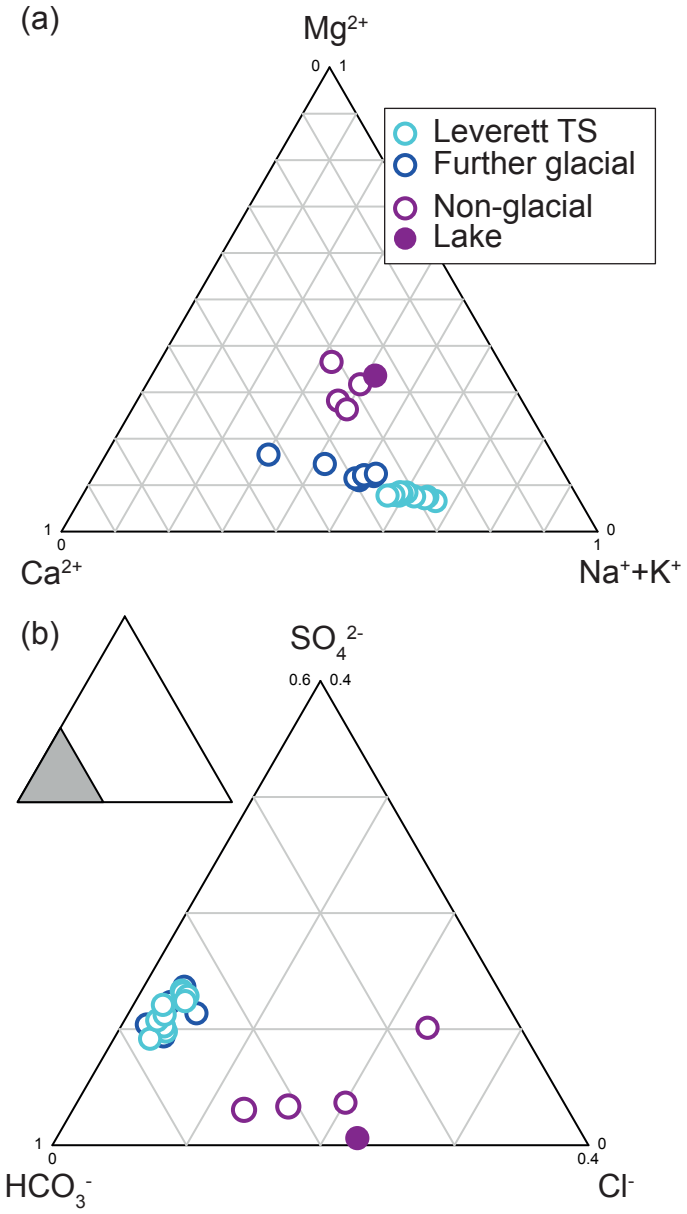
(a)
Mg2+
0
1
Leverett TS
Further glacial
Non-glacial
Lake
1
0
0
1
Ca2+
Na++K+
(b)
SO4 2-
0.6
0.4
1
0
0
0.4
HCO3-
Cl-

Fig. 3

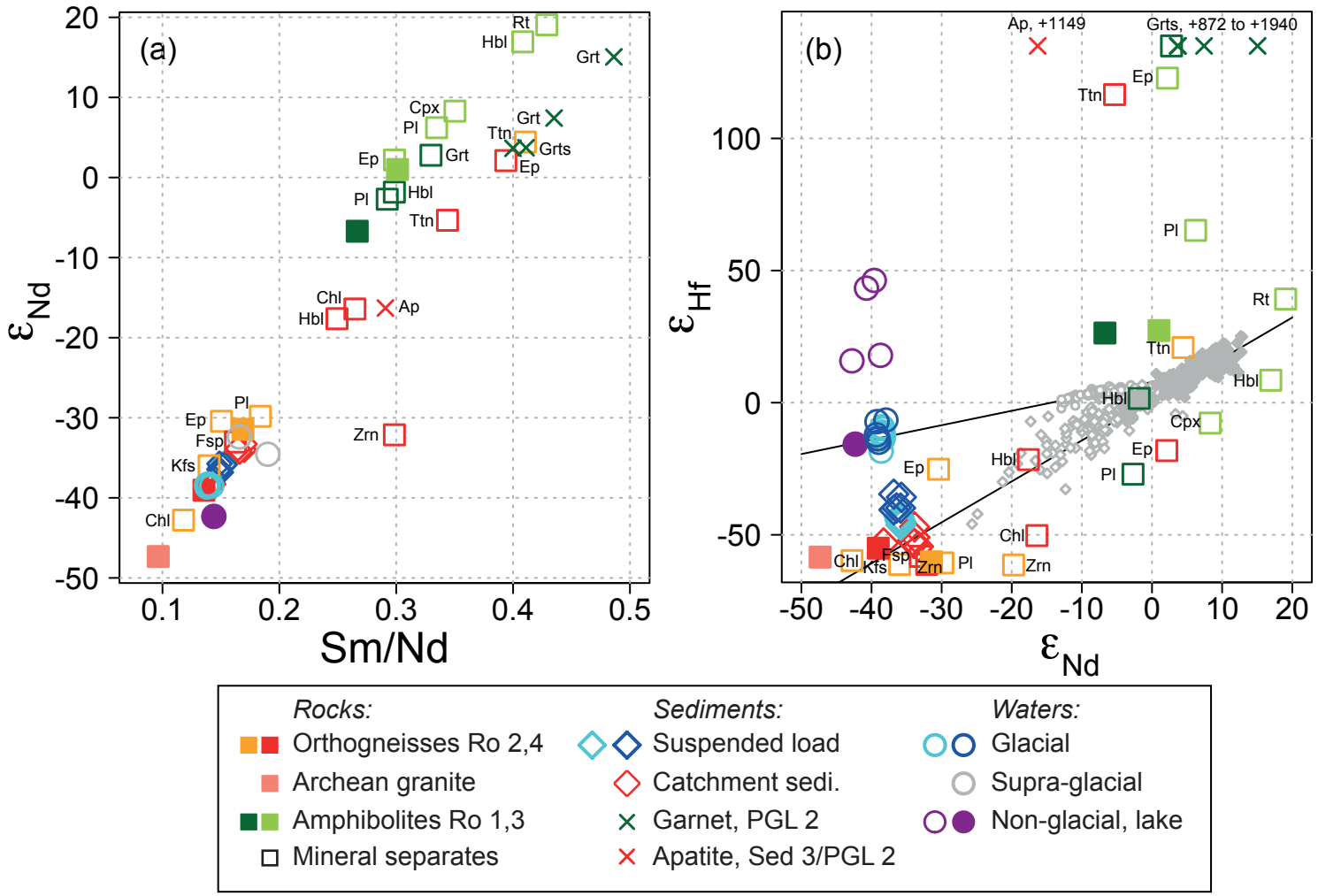
(a)
(b)
εNd
Sm/Nd
εHf
εNd
Rt
Hbl
Grt
Cpx
Pl
Ttn
Grts
Ep
Chl
Ap
Zrn
Fsp
Kfs
Ap, +1149
Grts, +872 to +1940
Rocks:
Orthogneisses Ro 2,4
Archean granite
Amphibolites Ro 1,3
Mineral separates
Sediments:
Suspended load
Catchment sedi.
Garnet, PGL 2
Apatite, Sed 3/PGL 2
Waters:
Glacial
Supra-glacial
Non-glacial, lake

Fig. 4

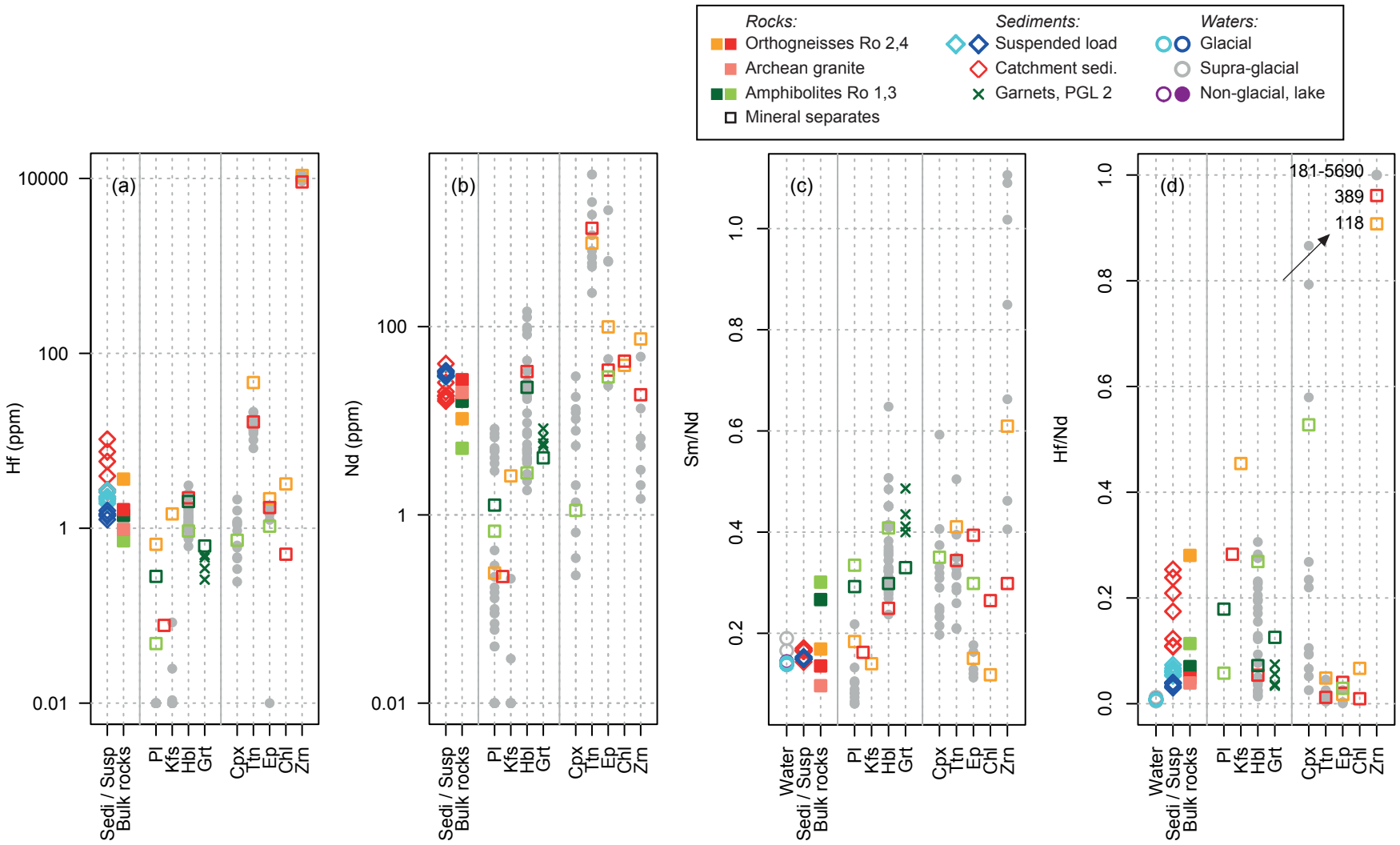
Rocks:
Orthogneisses Ro 2,4
Archean granite
Amphibolites Ro 1,3
Mineral separates
Sediments:
Suspended load
Catchment sedi.
Garnets, PGL 2
Waters:
Glacial
Supra-glacial
Non-glacial, lake
(a)
Hf (ppm)
10000
100
1
0.01
(b)
Nd (ppm)
100
1
0.01
(c)
Sm/Nd
1.0
0.8
0.6
0.4
0.2
(d)
Hf/Nd
1.0
0.8
0.6
0.4
0.2
0.0
181-5690
389
118
Water
Sedi / Susp
Bulk rocks
Pl
Kfs
Hbl
Grt
Cpx
Ttn
Ep
Chl
Zrn

Fig. 5

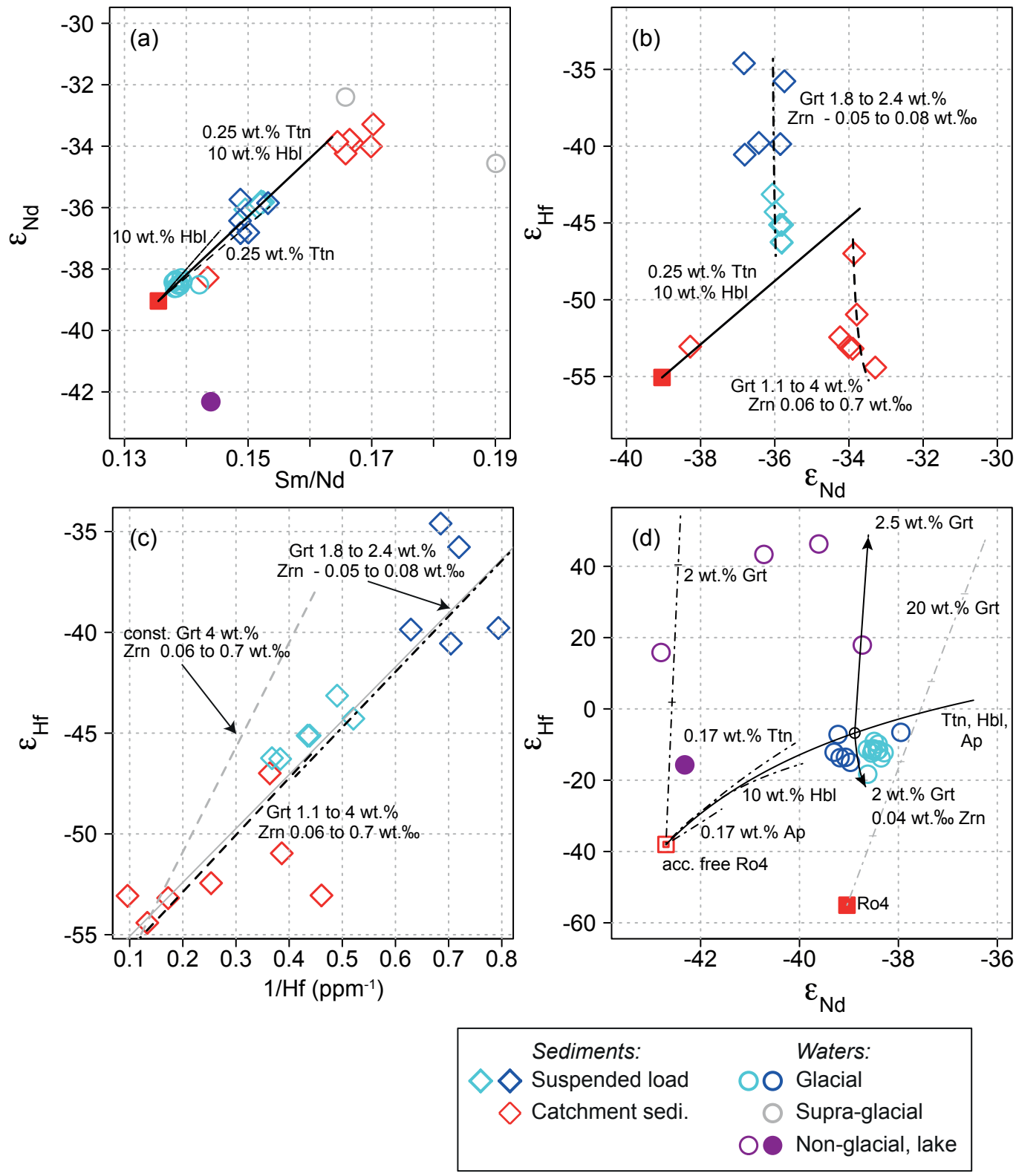
(a)
0.25 wt.% Ttn
10 wt.% Hbl
10 wt.% Hbl
0.25 wt.% Ttn
εNd
Sm/Nd
(b)
Grt 1.8 to 2.4 wt.%
Zrn - 0.05 to 0.08 wt.‰
0.25 wt.% Ttn
10 wt.% Hbl
Grt 1.1 to 4 wt.%
Zrn 0.06 to 0.7 wt.‰
εHf
εNd
(c)
Grt 1.8 to 2.4 wt.%
Zrn - 0.05 to 0.08 wt.‰
const. Grt 4 wt.%
Zrn 0.06 to 0.7 wt.‰
Grt 1.1 to 4 wt.%
Zrn 0.06 to 0.7 wt.‰
εHf
1/Hf (ppm-1)
(d)
2.5 wt.% Grt
2 wt.% Grt
20 wt.% Grt
Ttn, Hbl,
Ap
0.17 wt.% Ttn
10 wt.% Hbl
2 wt.% Grt
0.04 wt.‰ Zrn
0.17 wt.% Ap
acc. free Ro4
Ro4
εHf
εNd
Sediments:
Suspended load
Catchment sedi.
Waters:
Glacial
Supra-glacial
Non-glacial, lake

Fig. 6

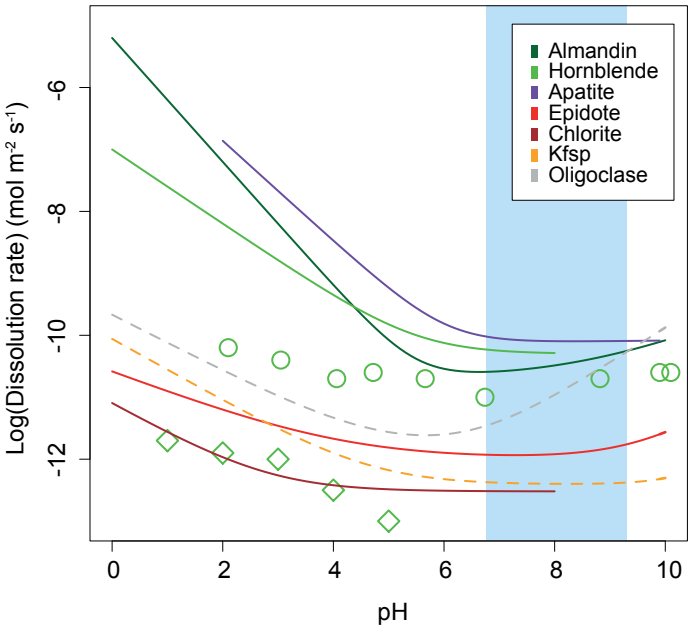
Almandin
Hornblende
Apatite
Epidote
Chlorite
Kfsp
Oligoclase
Log(Dissolution rate) (mol m-2 s-1)
-6
-8
-10
-12
0
2
4
6
8
10
pH

Fig. 7